Evidence for a Rapid Global Climate Shift across the Late 1960s

PETER G. BAINES

Department of Civil and Environmental Engineering, University of Melbourne, Melbourne, Australia, and QUEST, Department of Earth Sciences, University of Bristol, Bristol, United Kingdom

CHRIS K. FOLLAND

Hadley Centre, Met Office, Exeter, United Kingdom

(Manuscript received 3 November 2005, in final form 24 October 2006)

ABSTRACT

It is shown that a number of important characteristics of the global atmospheric circulation and climate changed in a near-monotonic fashion over the decade, or less, centered on the late 1960s. These changes were largest or commonest in tropical regions, the Southern Hemisphere, and the Atlantic sector of the Northern Hemisphere. Some, such as the decrease in rainfall in the African Sahel, are well known. Others appear to be new, but their combined extent is global and dynamical linkages between them are evident. The list of affected variables includes patterns of SST; tropical rainfall in the African Sahel and Sudan, the Amazon basin, and northeast Brazil; pressure and SST in the tropical North Atlantic and the west and central Pacific; various branches of the southern Hadley circulation and the southern subtropical jet stream; the summer North Atlantic Oscillation; south Greenland temperature; the Southern Hemisphere storm track; and, quite likely, the Antarctic sea ice boundary. These changes are often strongest in the June–August season; changes are also seen in December–February but are generally smaller. In Greenland, annual mean temperature seems to be affected strongly, reflecting similar changes in SST throughout the year in the higher latitudes of the North Atlantic. Possible causes for these coordinated changes are briefly evaluated. The most likely candidates appear to be a likely reduction in the northward oceanic heat flux associated with the North Atlantic thermohaline circulation in the 1950s to 1970s, which was nearly in phase with a rapid increase in anthropogenic aerosol emissions during the 1950s and 1960s, particularly over Europe and North America.

1. Introduction

Examination of the climate record shows examples of events where the climate underwent a change, or shift, between two identifiable "before and after" states. The term "climate shift" is preferred here to represent events that may be smaller or more regional than the commonly described global climate change. Recent studies (Alley et al. 2002, 2003) have warned of the potential for abrupt future climate change. In these reports, the most concrete examples given are from the distant past, such as the Younger Dryas, the mid-Holocene, and the Little Ice Age. Evidence is presented here that a much more recent example of an abrupt climate shift, though usually of considerably smaller but locally quite strong, magnitude may be identified in the past century, with present-day consequences. Specifically a substantial, coordinated, worldwide change occurred in a number of major climate variables over a period of about 10 yr, centered on the late 1960s. A range of examples are shown in Fig. 1. Some of these changes [such as the Sahel rainfall decrease, e.g., Dai et al. (2004)] are well known, some less so. Others have escaped widespread attention or have not been related to the wider behavior of the climate system, such as the pronounced interdecadal south Greenland temperature variations described by Chylek et al. (2006) also shown in Fig. 1 in a slightly different form. Some aspects of these coordinated changes as they affect southwest Australia have been described by Baines (2005).

The principal characteristics of these changes are that they were large, monotonic over the decade, and ap-

Corresponding author address: Peter Baines, Department of Civil and Environmental Engineering, University of Melbourne, Melbourne VIC 3010, Australia.
E-mail: p.baines@unimelb.edu.au

DOI: 10.1175/JCLI4177.1

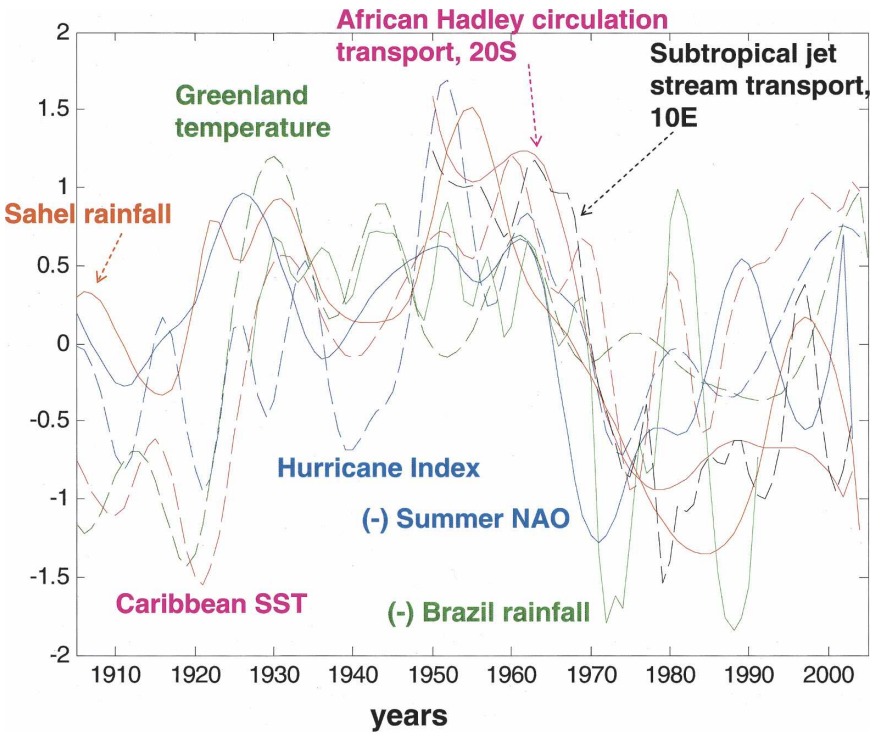

FIG. 1. Low-frequency variability of some of the principal variables that show the late 1960s climate shift for June–August (interannual variability has been removed, and data normalized by the mean and std dev of the original records). Details: Sahel rainfall (red): Hadley Centre data, 10°–20°N, 10°W–25°E; (−) Brazilian rainfall (green): University East Anglia data, 0°–10°S, east of 60°W; (−) southern node of summer NAO in July and August (blue): Hadley Centre sea level pressure data (Ansell et al. 2006); African Hadley circulation transport at 20°S (magenta): NCEP data, 20°W–20°E, 500–100 hPa; southern subtropical jet stream transport at 10°E (black dashed): NCEP data, 20°–40°S, 500–100 hPa; south Greenland (south of 65°N) coastal temperature (land and adjacent sea surface; dark green dashed) taken from HadCRUT3 (Brohan et al. 2006); SST over the south Caribbean (magenta dashed) taken from HadSST2 (Rayner et al. 2006), based on evidence given in Knaff (1997); and an index of intense hurricane activity over the North Atlantic (blue dashed) updated from Landsea et al. (1999).

proximately temporally coincident. In fact, the magnitude of the changes centered on the late 1960s makes them a key or dominant feature of each of their temporal records over the past 50 yr. The distribution of impacts is very widespread but more obvious in certain regions, such as the North Atlantic sector and the Tropics. Another example in the North Atlantic sector is a signature of this change in the sign of the summer North Atlantic Oscillation (NAO) pattern of anomalies of pressure at mean sea level (Hurrell and Folland 2002). This phenomenon operates mainly between northern Europe and the high Arctic in boreal summer, not dissimilarly to the well-known winter NAO pattern but with a smaller space scale and shifted northward [Fig. 1 of Hurrell and Folland 2002; Fig. 6 (June–August) of Hurrell et al. 2003; Fig. 8 of Greatbatch and Rong 2006]. Another relatively large signal can be seen in an index of the frequency of strong North Atlantic hurricanes, which occur in the season June to November (e.g., Landsea et al. 1999; Goldenberg et al. 2001). Other fluctuations on the interdecadal time scale are generally smaller in amplitude and the correlations between them are weaker. The global nature of this relatively abrupt climate shift has previously not been recognized because it occurred when the global coverage of climate data was patchy and incomplete, particularly in the Southern Hemisphere. It just precedes the observed minimum in the Northern Hemisphere and the global surface temperature around 1975 (Folland et al. 2001c). It is a separate and different phenomenon from the ENSO-like interdecadal climate shift dated around 1975 and centered on the Pacific, described by Zhang et

al. (1997), Folland et al. (1999), and many others. This is related to fluctuations in the Pacific decadal oscillation (Mantua et al. 1997) and its Pacific-wide manifestation, the interdecadal Pacific oscillation (Power et al. 1999).

We first describe the global nature and extent of the climate changes, followed by details of how some of them are connected. Attention is focused on the season June–August, when many changes are largest. A brief evaluation is then made of the possible causes. The atmospheric data used are primarily from the National Centers for Environmental Prediction–National Center for Atmospheric Research (NCEP–NCAR) reanalysis dataset (Kalnay et al. 1996; Kistler et al. 2001), which is broadly consistent (Trenberth et al. 2000) with the corresponding independent 15-yr European Centre for Medium-Range Weather Forecasts (ECMWF) Re-Analysis (ERA-15). The NCEP reanalysis is preferred to the 40-yr Re-Analysis (ERA-40) for tropical rainfall analyses, a central feature of this paper, as the latter is known to be sometimes very unreliable, but ERA-40 (Uppala et al. 2005) is used to check some key atmospheric circulation results. Reanalysis data have been supplemented by rainfall and surface records from other sources. The changes we describe are also manifest in SST, rainfall, pressure, and atmospheric circulation patterns. Note that periods have been identified in the literature where changes occurred in NCEP data that are not present in the atmosphere and these and their causes have been described by Kalnay et al. (1996) and Kistler et al. (2001). Fortunately these inhomogeneities appear to avoid our period of most interest. The most significant inhomogeneities occur in the late 1950s, with the expansion of the radiosonde network associated with the International Geophysical Year, and in the late 1970s, with the advent of the satellite era. Greatbatch and Rong (2006) specifically discuss these issues with respect to the Northern Hemisphere observations.

When examining time series, we have used the empirical mode decomposition procedure of Huang et al. (1998, 1999) to help identify the low-frequency component of the record. This simple procedure produces a high-frequency (interannual) component with zero local mean, which is subtracted from the original record to give the lower-frequency record. The procedure can be repeated several times to give a chosen frequency that separates high- and low-frequency behavior. In Fig. 1, it has been repeatedly applied two or three times to the annual time series for June–August (JJA) for each variable to give a low-pass filter with a cutoff period of near 5 yr to clearly show the multiannual to interdecadal variability.

2. Patterns of change in rainfall

Since tropical rainfall is a major driver of patterns of midlatitude weather, we consider this variable first. Corresponding changes in sea surface temperature (SST) are then described in the next section, followed by the consequent changes in atmospheric circulation. Global covariance empirical orthogonal functions (EOFs) have been constructed of precipitation in the Tropics (30°S–30°N) in the NCEP–NCAR reanalysis for several time periods. The EOFs have been computed using the singular value decomposition procedure, with algorithms provided by MATLAB. Attention is focused on the Northern Hemisphere summer season JJA. The mean worldwide rainfall for this season for the 10-yr period 1958–67 is shown in Fig. 2a to represent the mean state before the late 1960s shift. Taking the period 1948–2004 and removing the mean for the whole period, the first EOF of tropical rainfall anomalies explains 25.7% of the variance (Fig. 2b). The corresponding amplitude time series (Fig. 2c) shows a sharp increase centered on the late 1960s. The second, third, and fourth rainfall EOFs (not shown) explain variances of 8.8%, 6%, and 5.5%, respectively, with the third and fourth showing an El Niño–Southern Oscillation (ENSO)-like structure, and are not of direct interest here.

The spatial structure of the first EOF (Fig. 2b) shows strong negative values in three main regions: the Sahel of northern Africa, the Caribbean, and in the central equatorial Pacific. It also shows positive peaks in two main regions: the Amazon basin just south of the equator and over the Maritime Continent–Philippines north of the equator. These four regions constitute alternating maxima and minima spaced approximately 90° apart in longitude. The temporal record for this pattern (Fig. 2c) shows a sharp near-monotonic increase from near 1960 to the early 1970s, with a slower change in the same direction to the mid-1980s and with only relatively small interannual fluctuations superimposed. This substantial change captures the shape of the well-known decrease in rainfall in the African Sahel over just this period and implies that the changes in the other three main regions are approximately coincident and may be at least partly physically linked.

If this analysis is repeated for the main trend period, 1958–78, the results are very similar to those from 1948 to 2004. The first EOF has similar spatial structure to that shown in Fig. 2b, though the minimum in the central Pacific is not as strong. The overall time dependence is similar to that in Fig. 2c, though there are differences in the smaller fluctuations. Some changes and reordering are seen in the higher order EOFs, but

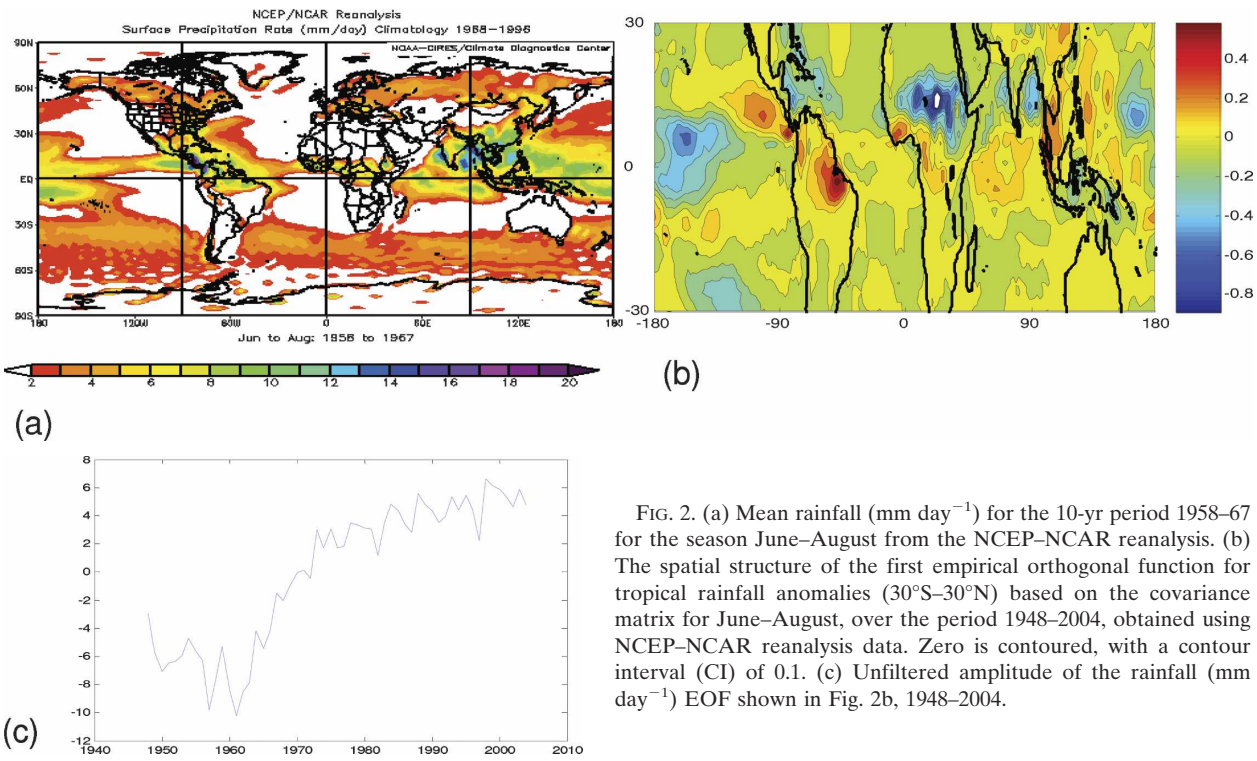

FIG. 2. (a) Mean rainfall (mm day^{-1}) for the 10-yr period 1958–67 for the season June–August from the NCEP–NCAR reanalysis. (b) The spatial structure of the first empirical orthogonal function for tropical rainfall anomalies (30°S–30°N) based on the covariance matrix for June–August, over the period 1948–2004, obtained using NCEP–NCAR reanalysis data. Zero is contoured, with a contour interval (CI) of 0.1. (c) Unfiltered amplitude of the rainfall (mm day^{-1}) EOF shown in Fig. 2b, 1948–2004.

these are not relevant here. If the analysis is repeated for the period 1979–2004, the first EOF described for the two periods above disappears as might be expected from the lack of trend in Fig. 2c in this period. The pattern shown in Fig. 2b cannot be identified with any of the first three 1979–2004 EOFs. EOF1 now resembles EOF2 for 1948–2004 and has an identifiable ENSO-like structure and time series.

If the analysis is repeated for the December–February (DJF) rainfall instead of JJA, for the periods 1948–2004 and 1958–78, the first EOF resembles that for JJA shown in Fig. 2b (as described later in section 4). The time series for the latter contains the major change shown in Fig. 2c, but the magnitudes are smaller and spread out over a longer time interval. If these analyses are repeated for the whole year, the first EOF has a structure and temporal variation that resembles that shown in Figs. 2b and 2c, which implies that the JJA changes dominate the annual picture.

In summary, the NCEP–NCAR reanalysis precipitation data show that there was a major change in the global pattern of rainfall in June–August centered on the late 1960s, which tended to persist throughout the year. This major change is approximately coincident with the well-known rainfall decrease in the African Sahel, but the pattern contains major changes in other regions of the Tropics. This coordinated change was unique in its magnitude and large-scale structure over the past 50 yr. It commenced near 1961 and was largely complete by 1973. This pattern of change (Fig. 2b) does not seem to be prominent in more recent variations.

The NCEP–NCAR rainfall data have been used here because they provide global coverage. These data have the disadvantage that they are derived quantities and are thus less reliable than the directly measured meteorological variables, such as pressure and temperature. The main results may be compared with an analysis by Lau and Sheu (1990), who derived EOFs from rainfall data from 155 stations over the period 1901–80. These data are real rainfall but suffer from the deficiencies of a sparse network. Lau and Sheu (1990) described three EOFs for annual mean data. The first of these was related to ENSO. The second contained interdecadal variability and appeared to be related to the Indian/Asian monsoon. The third had a structure that resembled Fig. 2b, though without the major peak in the African Sahel because of a deficiency in stations there. The temporal behavior of their EOF3 showed a similar long-term trend to that of Fig. 2c. Hence it appears that the large-scale change is represented in both datasets, each with its different shortcomings.

3. Patterns of change in sea surface temperature

Large-scale patterns of SST change over the past century have been described by Folland et al. (1999) and

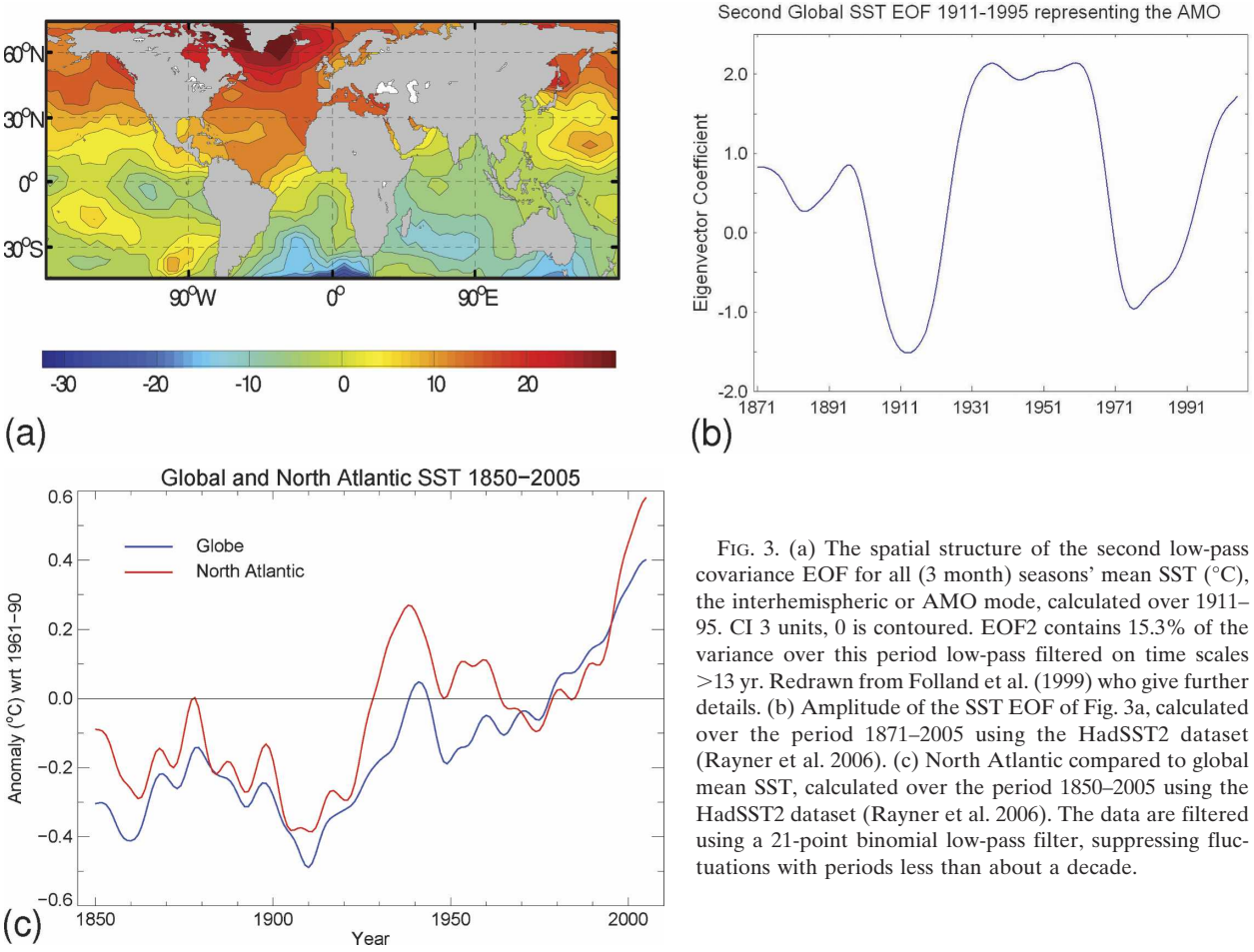

FIG. 3. (a) The spatial structure of the second low-pass covariance EOF for all (3 month) seasons' mean SST (°C), the interhemispheric or AMO mode, calculated over 1911–95. CI 3 units, 0 is contoured. EOF2 contains 15.3% of the variance over this period low-pass filtered on time scales >13 yr. Redrawn from Folland et al. (1999) who give further details. (b) Amplitude of the SST EOF of Fig. 3a, calculated over the period 1871–2005 using the HadSST2 dataset (Rayner et al. 2006). (c) North Atlantic compared to global mean SST, calculated over the period 1850–2005 using the HadSST2 dataset (Rayner et al. 2006). The data are filtered using a 21-point binomial low-pass filter, suppressing fluctuations with periods less than about a decade.

Cai and Whetton (2001); the latter gives results broadly similar to the slightly different Folland et al. analysis. Cai and Whetton calculated covariance EOFs of unfiltered annual mean SSTs for the period 1880–1997 using version 3 of the Global Sea Ice and SST dataset (GISST; Rayner et al. 1996). EOF1, with 43.6% of the total temporal variance, was identified with global warming, and EOF2 had 12.2% of the total variance and was identified with both the interannual and interdecadal variations of ENSO. EOF3 had 7.1% of the total variance, was identified with interhemispheric differences in temperature, and is our main concern here. This EOF showed a rapid decrease of the mean temperature of the Northern Hemisphere over the late 1960s.

We have used Folland et al.'s (1999) low-pass covariance EOFs here, calculated using the anomaly data for all seasons for the period 1911–95. Anomalies are calculated from a 1961–90 average and a low-pass filter near 13 yr is used. The region south of 45°S is largely excluded because of a lack of data, as is also the region north of 65°N because there the ocean is mostly covered with ice. EOF1 corresponds to global warming as expected, explaining 45.5% of the low-pass variance. EOF2 (Fig. 3a) corresponds to the interhemispheric pattern that looks much like the Atlantic multidecadal oscillation (Delworth and Mann 2000; Knight et al. 2005, 2006). This explains 15.3% of the low-pass variance. EOF3 (12.7% of the low-pass variance) corresponds to the interdecadal Pacific oscillation of Power et al. (1999) and is thus the global manifestation of the Pacific decadal oscillation (Mantua et al. 1997), as shown by Folland et al. (2002). EOF2 indicates a quasi-symmetric contrast between the Northern and Southern Hemispheres, and it is present in slightly different forms in different datasets or analyses (e.g., Mann and Park 1994; Enfield et al. 2001). The main problem is to avoid epochs and analyses where the eigenvalues of EOF2 and EOF3 are similar, as can easily happen, as confounding between their patterns can then occur. We also prefer to use a dataset that does not use EOFs in its construction, so we have excluded the Hadley Centre

Sea Ice and SST dataset (HadISST; Rayner et al. 2003). The mode in Fig. 3a is termed the "interhemispheric mode" by Cai and Whetton (2001) and is similar to the SST pattern identified by Folland et al. (1986) as being correlated with interdecadal variations in Sahel rainfall over the twentieth century. The phasing of the fluctuations in North Atlantic SST is also like that of the pattern of interdecadal SST variation found by Kushnir (1994). From now on we will refer to this as the Atlantic multidecadal oscillation (AMO; Delworth and Mann 2000). Note, however, that (a) the zero line in the Atlantic is on average near 10°S rather than on the equator, similar to Cai and Whetton (2001), (b) the amplitude is larger in the Atlantic than the Pacific, and (c) the amplitude in the Southern Hemisphere is appreciably smaller overall than that in the Northern Hemisphere. The time series for the AMO mode is shown in Fig. 3b, calculated using the newly enhanced noninterpolated Second Hadley Centre SST dataset (HadSST2; Rayner et al. 2006) and adjusting the time series for data gaps using the procedure of Folland et al. (1999). This differs in relatively minor details from that in Folland et al. due to improved data coverage. It indicates a substantial and sharp change centered on the late 1960s and mostly occurring over the period 1960–75. Thus the ocean surface in the Northern Hemisphere cooled in the late 1960s relative to the Southern by a magnitude that increased with latitude north of 10°S to up to relative amounts of about 1°C close to Greenland (e.g., as shown by decadal maps in Parker et al. 1994). This change was the reverse of a subsequent and almost equally large rise over the 20-yr period 1985–2005 and an earlier and even larger rise from about 1915 to 1935. It is important to emphasize that the global warming component of long-term SST change is not present in Fig. 3a. Thus the North Atlantic has recently warmed considerably more than implied by EOF2 due to a superimposed global warming component that is present in most of the World Ocean. As a result of the AMO and global warming working in concert, the North Atlantic has warmed substantially faster than the oceanic global average since 1985 (Fig. 3c). In the North Atlantic average, a warming influence of the AMO is evident in the middle of the twentieth century as is a sharp reduction in SST in the 1960s. Since 1985, overall warming of the North Atlantic has taken its mean SST about 0.3°C above the peak near 1940. However, according to the EOF2 time series, the contribution of the AMO is insufficient on its own to cause warming of the North Atlantic above the mid-twentieth-century peak by 2005. The recent relatively rapid global warming therefore significantly influences the interpretation of at least a few of the curves shown in Fig. 1 in recent decades, as discussed in section 5. However, global warming was likely to have been too slow to really influence SST changes centered on the 1960s anywhere, as also indicated by Fig. 3c.

The change in the late 1960s shown in Fig. 3 includes a general slight cooling in the tropical oceans, and in particular, in the central Pacific, centered on about 20°N, 140°W. The cooling in this central Pacific region corresponds to the decrease in rainfall in the same region shown in Fig. 2. A similar correlation is also evident in the tropical Atlantic, where cooler temperatures west and northwest of the Sahel correspond with reduced rainfall in the same region and increased rainfall to the south. Inspection of Figs. 2 and 3 indicates that the reduced SST implied by Fig. 3 tends to correspond with reduced rainfall elsewhere in the tropical oceans, though the correlation is far from perfect. Note that changes in the interdecadal Pacific oscillation–related EOF3 were relatively small in the late 1960s, so it probably had only small regional effects.

Changes in tropical SST over the late 1960s for different seasons have been assessed by taking differences between means for the two periods 1958–67 and 1976–95 for both June–August and December–February. This shows that the pattern of changes in each season is broadly similar to that shown in Fig. 3a, with the Southern Ocean warming and the northern oceans cooling, including cooling in the central equatorial Pacific near 160°W. Although global warming affects this SST analysis, it does this by a fairly similar amount in each hemisphere overall (Folland et al. 2001c). The changes in June–August also are slightly larger in magnitude than those for December–February (not shown here).

4. Changes in large-scale winds and other variables

We first describe changes in the meridional wind field for JJA in the upper troposphere, represented by the 200-hPa level. In the Tropics, the main region of interest, this flow is dominated by the upper branch of the Hadley circulation. Many of the details of these flows have been described for the 1979–93 period by Trenberth et al. (2000). The southward flow at this level is concentrated longitudinally in four regions, shown in Fig. 4a, which can be related to the regions of maxima in precipitation north of the equator, for this season, as follows. The first region or branch of the Hadley circulation is the African branch, whose core lies just to the west of the African continent south of 5°N, and is fed by the latent heat release associated with the rainfall maximum in north tropical Africa, known as the North African summer monsoon. The second branch extends southward across the Indian Ocean and is fed by the

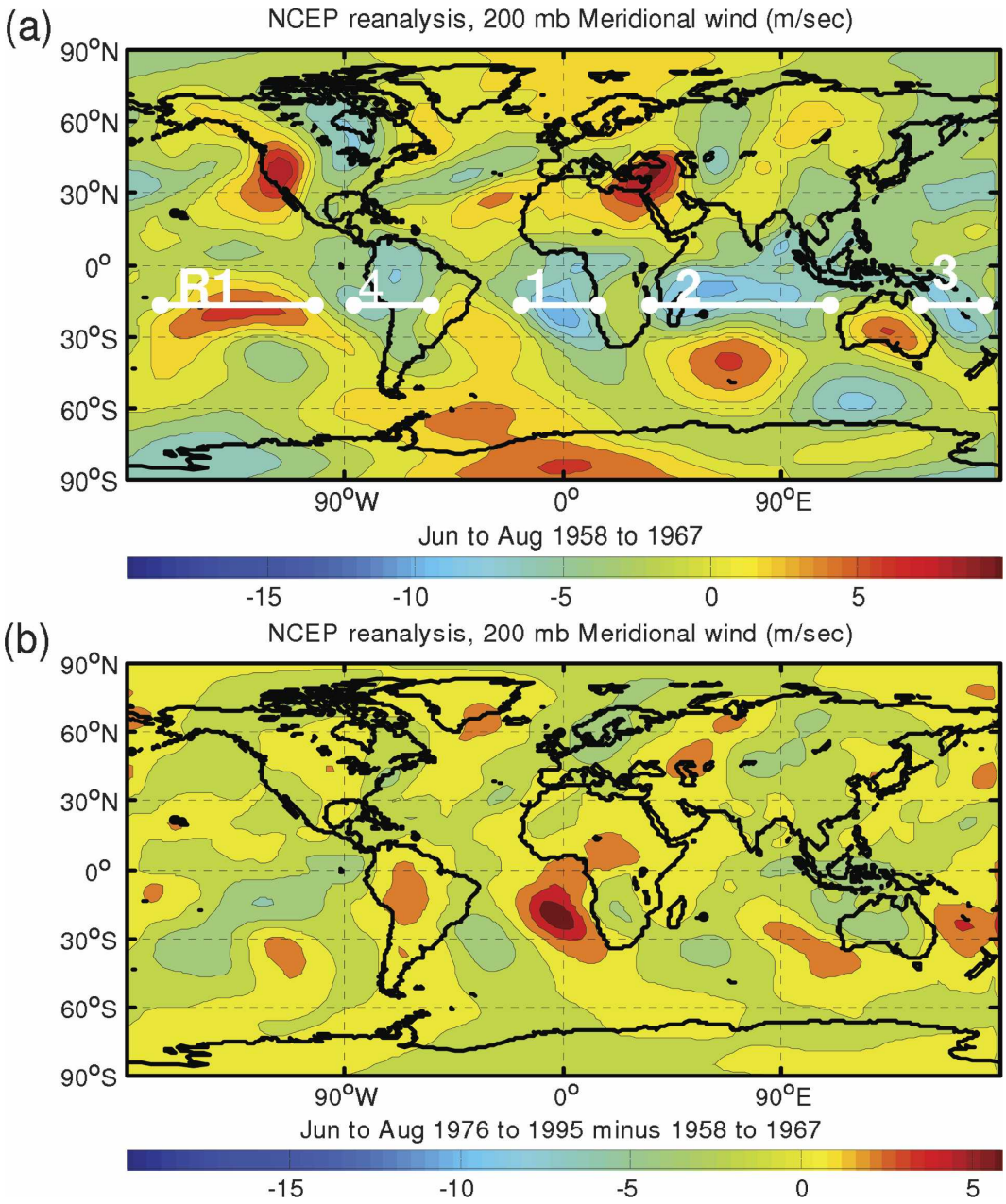

FIG. 4. (a) Mean meridional wind field at 200 hPa for June–August for the period 1958–67. White lines at 15°S denote sections across the four southward branches of the Hadley circulation (numbered in white, eastward from Greenwich) and the reversed (northward) Hadley circulation in the east Pacific, labeled R1. (b) The mean meridional wind field at 200 hPa for June–August for the period 1976–95, relative to the period 1958–67. CI 2 m s^{-1}, 0 is contoured in both figures.

Indian and Southeast Asian monsoon. The third branch is contiguous with the second and extends southward east of the Australian continent toward New Zealand. The fourth branch extends southward over and just west of South America, from the region of the rainfall maximum near the Caribbean. Of these four branches, the broadest and strongest is the second, associated with the Indian and Southeast Asian monsoon. Between these branches of the Hadley circulation, there are reverse flows at 200 hPa, which subtract from the overall net zonal mean transport southward. The largest of these occurs in the central Pacific east of the date line, between the third and fourth branches, where there is an anomalous region of northward flow at 200

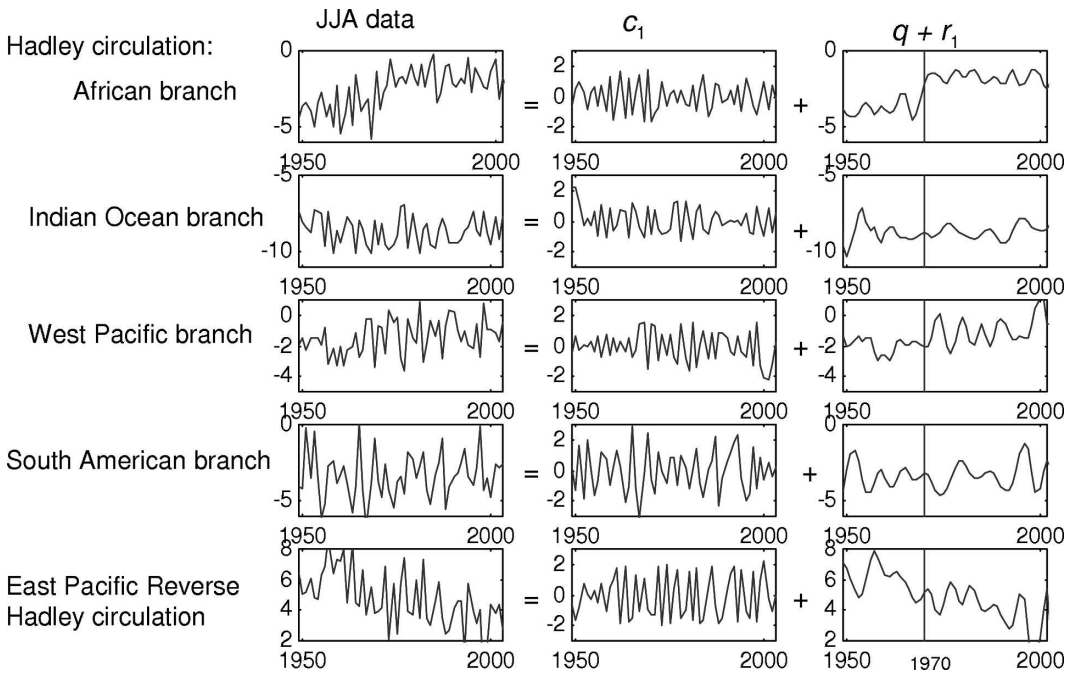

FIG. 5. Mean transport (10^{10} kg m s^{-1}) across the five sections at 15°S marked in Fig. 4a. (left) The data with one point per year for JJA. (middle) The interannual variability, according to the empirical mode decomposition of Huang et al. (1998, 1999); the curves in this column have zero local mean. (right) The residual low-frequency behavior or difference between columns 1 and 2. The vertical dashed line denotes the year 1970.

hPa in Fig. 4a, implying a reverse Hadley circulation. There are other smaller regions of reversed Hadley circulation over Australia and the western South Atlantic Ocean. The northward return flows in the Hadley circulation in the lower troposphere are generally much more spread out and less conspicuous, except for the return flow in branch two in the Indian Ocean sector, which is concentrated in the Somali jet (e.g., as described by Gill 1982). The southward return flow in the reverse Hadley circulation in the east central Pacific is relatively coherent and situated approximately beneath the upper-level northward flow.

The changes in the upper-level meridional velocity across the late 1960s, as inferred from the NCEP–NCAR reanalysis, are illustrated in Fig. 4b, which shows the meridional wind field averaged over the 20-yr period 1976–95, relative to 1958–67 (i.e., as in Fig. 4a). This long averaging time shows that the changes are quite long lasting. If the average is instead taken over the period 1971–80, the result is very similar to Fig. 4b. Figure 5 shows the time series of the transports in the upper-level components of the four branches of the Hadley circulation and the east Pacific reverse at 15°S, integrated over the height range from 500 to 100 hPa, with longitude ranges as marked in Fig. 4a. With regard to the change centered on the late 1960s, a major decrease is seen to occur in the transport of the first (African) branch in the Hadley circulation that is visibly connected with the well-known decrease in the rainfall in the African Sahel. This implies a reduced southward flux of heat in this longitude sector. There were no substantial coincident changes in the transports in the second (Indian Ocean) or the fourth (American) branches. There is an apparent small decrease in the strength of the third branch and a significant decrease in the strength of the reverse Hadley circulation in the east Pacific. When reductions occur in the transport in these Hadley circulation branches, they imply a reduced southward heat transport in their respective longitude bands.

One may expect to find a close correlation between the time series of the rainfall of a particular tropical region, and the transports of a branch of the Hadley circulation that emanates from it. This is the case for Sahel rainfall and the African branch of the Hadley circulation. It does not apply to Amazon rainfall in JJA, since this region is south of the equator and displaced from the center of the main source of the South American branch, which is near Central America and the Caribbean. Furthermore, the decreased northern transport in the east Pacific reverse branch of the upper-level Hadley circulation (Fig. 4b) appears to be related to the reduced eastward transport in the southern subtropical jet stream that feeds it (Fig. 6b), as it accom-

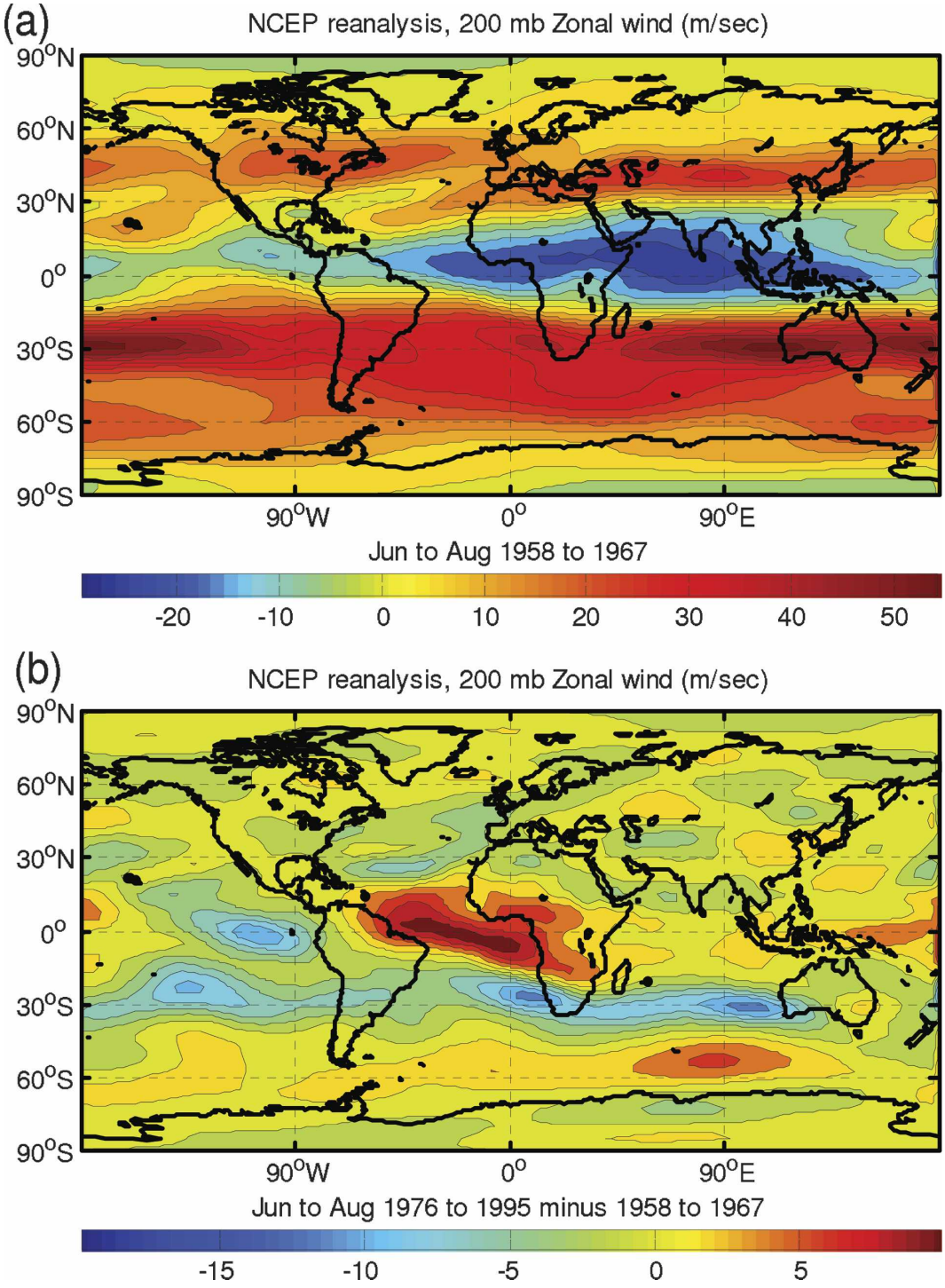

FIG. 6. (a) Mean zonal wind at 200 hPa for June–August for the period 1958–67 from NCEP–NCAR reanalysis, CI 5 m s^{-1} and 0 is contoured. (b) Same as in (a), but showing the difference between the period 1976–95 and 1958–67, CI 2 m s^{-1}.

panies a decrease in rainfall in the north-central Pacific at its downstream end (Fig. 2b). Table 1 shows the correlation coefficients between the five transport curves of Fig. 5, and the Southern Oscillation index (SOI), for the years 1949–2002. For the SOI, the mean value for the period June–August for each year is taken and is included to give a measure of the connection of these transports with the ENSO. Values for the interannual

TABLE 1. Correlation coefficients (CCs) between the transports in the four branches of the southern Hadley circulation, the east Pacific reverse, and the SOI for the season June–August over the period 1949–2002. In each group, the first item is for the whole record, the second is for the first high frequency record (IMF), denoted c_1, and the third is for the low-frequency remainder, $q + r_1$. Coefficients of 0.3 or greater (significant at 40 degrees of freedom) are shown in bold italics.

CC values for total c_1, $q + r_1$	Transport—African branch	Transport—Indian branch	Transport—West Pacific branch	Transport—South American branch	Transport—East Pacific reverse	SOI
Transport—African branch	1	−0.04	0.19	−0.02	***−0.56***	−0.07
	1	0.09	0.02	−0.11	***−0.38***	0.13
	1	0.09	***0.50***	−0.06	***−0.64***	−0.20
Transport—Indian branch	−0.04	1	***−0.48***	0.12	0.08	0.24
	0.09	1	***−0.30***	0.06	−0.08	−0.21
	0.09	1	0.00	0.15	−0.18	−0.06
Transport—West Pacific branch	0.19	***−0.48***	1	***−0.35***	***−0.62***	***0.64***
	−0.02	***−0.30***	1	***−0.30***	***−0.53***	***0.58***
	0.50	0.00	1	−0.14	***−0.66***	0.13
Transport—South American branch	−0.02	0.12	***−0.35***	1	−0.06	***−0.55***
	−0.11	0.06	***−0.3***	1	−0.1	***−0.50***
	−0.06	0.15	−0.14	1	0.06	−0.18
Transport—East Pacific reverse	***−0.56***	0.08	***−0.62***	−0.06	1	−0.23
	−0.38	−0.08	***−0.53***	−0.1	1	***−0.38***
	−0.64	−0.18	***−0.66***	0.06	1	0.06
SOI	−0.07	0.24	***0.61***	***−0.55***	−0.23	1
	0.13	−0.21	***0.58***	***−0.50***	***−0.38***	1
	−0.20	−0.06	0.13	−0.18	0.061	1

(c_1) and the residual low-frequency variation ($q + r_1$) have also been calculated and are shown in the second and third row, respectively, in each box of Table 1. The reverse Hadley circulation in the east Pacific is strongly correlated with the African and west Pacific branches for all three rows but not the other two branches. The Indian Ocean branch is inversely correlated with the west Pacific branch at interannual frequencies but not at low frequency ($q + r_1$). The South American and west Pacific branches are correlated at low frequency. The SOI is significantly correlated with the three Pacific branches (west, American, and reverse) at interannual frequencies but not at low frequencies. This implies, as one would expect, that variations in these transports are significant for ENSO. These data support the impression from Figs. 4 and 5 that the late 1960s change is manifest in the African and west and central Pacific branches of the JJA Hadley circulation but not in the Indian and American branches.

The mean zonal winds at 200 hPa for the period 1958–67 for JJA are shown in Fig. 6a. This flow consists of weak easterlies near the equator, a strong westerly subtropical jet stream near 30°S with a maximum over Australia and the west Pacific, and a much weaker westerly jet near 40°N, strongest over central Asia. These subtropical jet streams with large longitudinal extent effectively owe their existence to the conservation of angular momentum of upper-level air carried poleward by the various branches of the Hadley circulation and are seen to vary in intensity along their length with the poleward north–south flows on their equatorward side. Figure 6b shows the mean zonal flow at 200 hPa for the 20-yr period 1976–95, relative to the period 1958–67, for JJA. This shows the principal features of the late 1960s change in upper troposphere zonal flow. The anomalous zonal flows near the equator represent Walker-type circulations that are consistent with low (or zero) frequency Kelvin wave response forced by changes in the latent heating from the rainfall anomalies described in section 2 (Gill 1980), with an approximate zonal wavenumber-2 pattern. For the subtropical jet stream near 30°S, there is a substantial decrease in velocity at nearly all longitudes. This is generally consistent with the changes in the Hadley circulation that drive the jet stream and includes the reverse Hadley circulation in the central Pacific east of the date line, which becomes less intense after the late 1960s, as described above. The positive zonal flow anomaly extending southeastward across the South Atlantic Ocean and southern Africa is related to the increased rainfall in the Amazon basin, and this partly offsets the decreased contribution to the subtropical jet stream from the African Hadley circulation. At the 850-hPa level, representative of the lower troposphere, in the Atlantic and Indian Ocean sectors the main storm-track region of strong zonal winds moved south by a distance of order 0.5° latitude (not shown here; see Baines 2005). In physical terms, this may be interpreted as a conse-

quence of the reduced meridional heat flux through this range of longitudes, so that the environment south of 30°S is less baroclinic and hence less unstable; the simple two-layer criterion for baroclinic instability (Phillips 1954) then implies that the eddies should form farther poleward where the beta effect is weaker (Baines 2005).

This type of behavior is mirrored in the Northern Hemisphere. In Fig. 4a, there is a (relatively) weak JJA northward branch of the Hadley circulation from the African monsoon, centered on 30°N, 30°W, and Fig. 4b indicates that this northward transport of heat also decreased after 1970. Consistent with this, the North Atlantic storm track (as marked by zonal winds at 850 hPa; not shown here) moved north, as did the upper-level jet stream as shown in Fig. 6b. This storm-track variability is closely related to the phase of the summer North Atlantic Oscillation (Hurrell and Folland 2002). This indicates that a significant northward displacement of this storm track occurred centered around 1970, after which the summers in much of the United Kingdom and other parts of northwest Europe were generally warmer and dryer than previously (C. K. Folland et al. 2007, unpublished manuscript). This corresponds to increased anticyclonic conditions in the southern node of the North Atlantic Oscillation over northwest Europe and increased cyclonic conditions over the high latitudes of the Atlantic sector in the northern node. Hence, the picture of the dynamical changes occurring during JJA across the late 1960s is generally consistent with known atmospheric dynamics and is forced by the associated changes in latent heating that drive the Hadley circulation. This may largely explain the similar decadal behavior of the summer NAO and Sahel rainfall in Fig. 1 over the last century, and particularly summer (July–August) rainfall over southern England and summer Sahel rainfall when these rainfall data are standardized (see Fig. 10).

Figures 4b and 6b lie at the heart of our analysis. To check the veracity of the results, we have carried out the same 200-hPa analysis for JJA using ERA-40 data (Figs. 7a–d). The maps of mean u and v for 1958–67 are generally quite similar, particularly in the Atlantic sector. The maps of v for 1976–95 minus 1958–67 also have a similar pattern in the Atlantic sector. Greater differences are seen elsewhere, for example, over Australia; despite this, there appear to be no gross differences of sign anywhere in the larger-scale patterns. Our findings using the NCEP data concerning changes in the v component of the Hadley circulation in the Atlantic sector are well verified by the ERA-40 data. The striking changes in u between 1976–95 and 1958–67 are also well reproduced in ERA-40 almost globally, with a pronounced reduction in the strength of the Southern Hemisphere subtropical jet stream. However, the reduction seen in the NCEP analysis over southwest Western Australia only reaches the west coast of that region in ERA-40. Overall, however, we consider that the two analyses support each other well.

So far we have described the dynamical and atmospheric circulation changes that occurred during the season June–August. The changes that occurred across the late 1960s in other seasons were not as large. For the season September–November (SON), the climatology of the variables described above is generally similar to that for June–August, but the magnitudes of rainfall, the Hadley circulation, and subtropical jet stream speeds are generally smaller. Hence the changes shown in Figs. 3–7 may be taken as representative of the nature of the changes for 6 months of the year, from June to November.

The atmospheric circulation changes in the Northern Hemisphere winter season (DJF) are also generally smaller than those for the summer season, and some of them are shown here for completeness and comparison. Figures 8a and 8c show the mean meridional and zonal winds at 200 hPa for DJF for the period 1958–67, corresponding to Figs. 4a, 6a, 7a, and 7c. Again, there are three main branches of the Hadley circulation, but located now in the Northern Hemisphere, emanating from the main rainfall regions over land south of the equator as shown in Fig. 9a: Africa, the Southeast Asian monsoon, and from Central America. These are separated by three reverse Hadley circulations, the largest being over the central North Pacific. In the Southern Hemisphere, the various branches of the Hadley circulation described for JJA are still identifiable but are much reduced in magnitude. For the zonal flows (Fig. 8c), there are weak easterlies spanning a broad range of latitudes over the equator, everywhere except the central Atlantic and the east Pacific. The northern subtropical jet stream is prominent, fed by the African and Southeast Asian branches of the Hadley circulation. There are significant (up to 30%) changes in precipitation in Africa, South America, the central Pacific, and Southeast Asia, as indicated in section 2. This is identified by the first EOF of tropical rainfall anomalies in DJF in Fig. 9b. The time series of this EOF is shown in Fig. 9c and shows a steady increase through the 1960s and 1970s. The associated wind changes at 200 hPa for DJF for 1976–95 minus 1958–67 are shown in Figs. 8b and 8d. If the rainfall is differenced in the same way, it shows a similar pattern to that of the EOF in Fig. 9b.

Figure 8d shows that the changes in the Walker cir-

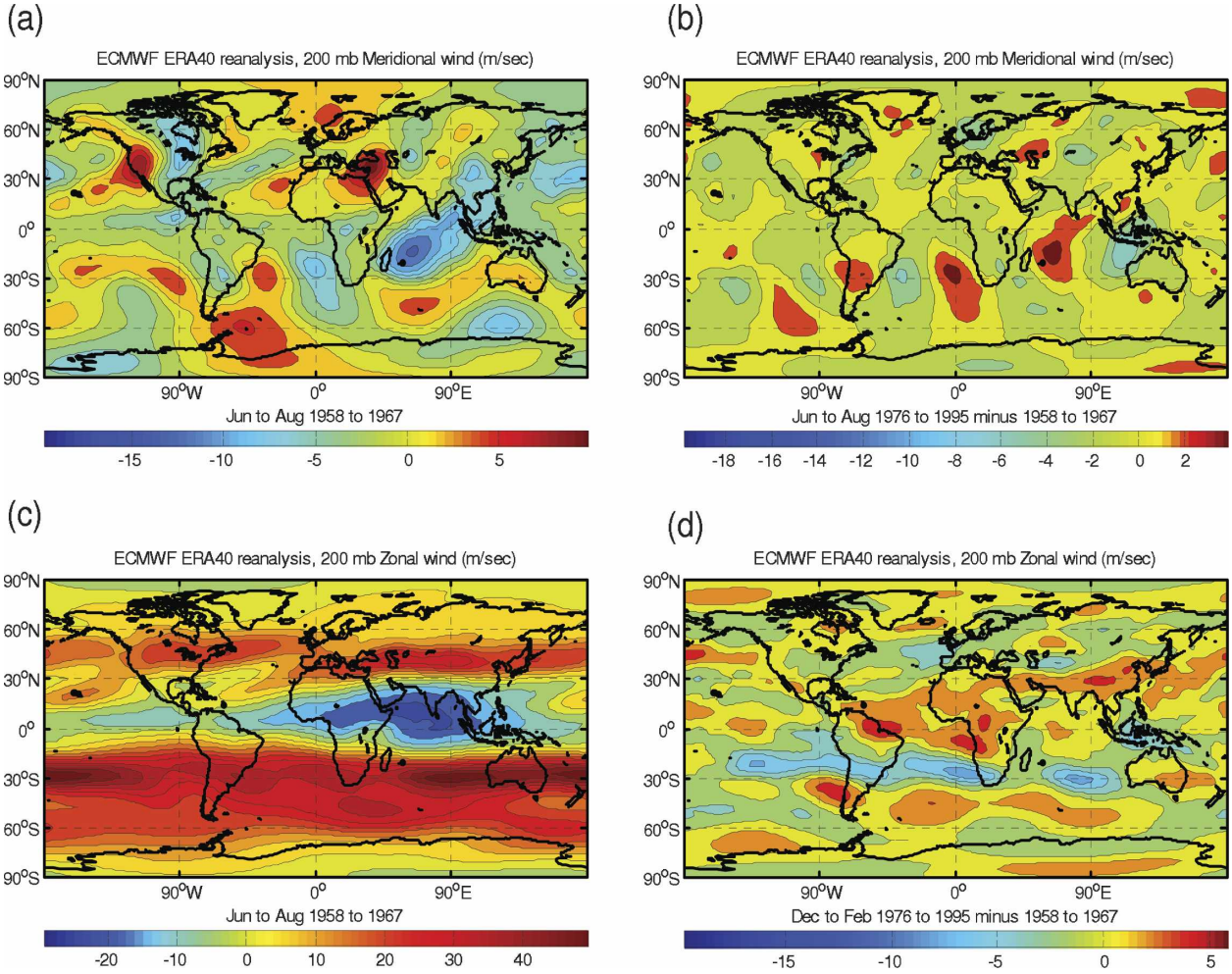

FIG. 7. Winds at 200 hPa for June–August, same as in Figs. 4 and 6, but for the ECMWF ERA-40 reanalysis. (a), (b) Meridional winds same as in Figs. 4a and 4b, CI 2 m s^{-1}, 0 contoured and (c), (d) zonal winds same as in Figs. 6a and 6b, CI 2 m s^{-1}.

culation have large eastward components over the Atlantic and Southeast Asian sectors, which can be related directly to the rainfall increases over South America and the central Indian Ocean. The changes in the Hadley circulation (Fig. 8c) do not all coincide with the main branches shown in Fig. 8a. The African branch of the northern Hadley circulation (0° longitude) is reduced in 1976–95, but there is an increase in northward motion in the western Indian Ocean (60°E), and these changes are reflected in the changes seen in the northern subtropical jet stream near 30°N (a decrease in velocity centered on 0° longitude and an increase near 60°E) in Fig. 8d. In the Southern Hemisphere, the African branch of the southern Hadley circulation again decreases across the late 1960s, though less than in JJA. However, the main storm track in the southern Indian Ocean sector still moves south, as the negative shading north of 45°S and positive shading south of 45°S in the Indian Ocean longitudes in Fig. 8d indicate. The corresponding changes for the season March–May (MAM) are smaller but broadly similar to these.

There are other Southern Hemisphere variables that show significant changes across the late 1960s. One of these is the rainfall of southwest Western Australia, which mostly falls in June–August. This suffered a 20% long-term decrease centered on the late 1960s. This decline has had significant economic consequences for the region, and the cause has been sought for some time (IOCI 2002; Smith et al. 2000; Timbal et al. 2006). This rainfall decrease now appears to be a consequence of the large-scale atmospheric circulation changes in June to August described above and is attributed locally to the southward movement of the storm track near southwest Western Australia. This can be traced back to the rainfall reductions in the North African monsoon and thus in the Sahel and regions just to the south (Baines

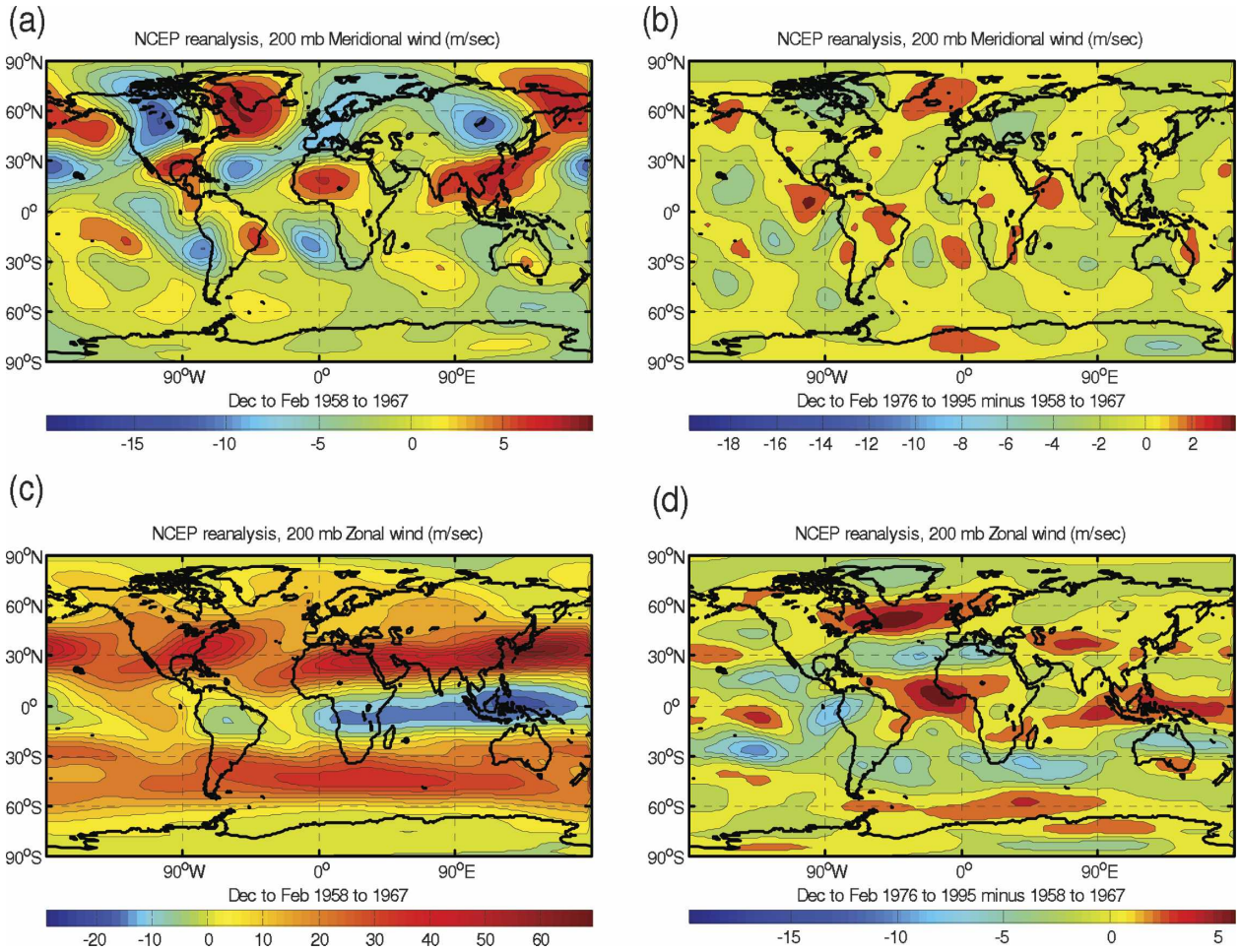

FIG. 8. NCEP–NCAR reanalysis winds at 200 hPa, same as in Figs. 4 and 6, but for the season December–February. (a), (b) Meridional winds CI 2 m $s^{-1}$and (c), (d) zonal winds CI 5 m s^{-1}, 0 contoured.

2005) and so back, at least in part, to the AMO SST pattern. The Sahel and southwest Western Australian rainfall curves are shown together in Fig. 10 with that for southeast England, which was maximally affected by the phase changes in the southern node of the summer NAO. Figure 10 is a remarkable example of a common global-scale influence on regional climate in three areas very far apart.

Another Southern Hemisphere change concerns the latitude of the edge of the southern pack ice in summer (DJF), inferred from whale catch records (de la Mare 1997). Although data are missing from the decade of the 1960s, there is clearly a substantial southward movement across this period. There were little data on SST in high southern latitudes at that time, but this change clearly indicates a zonal mean increase in SST in the region between the two extreme latitudes of the ice edge, again centered on the late 1960s. It is consistent with reduced baroclinicity in mid- to high southern latitudes after this date, at least in summer, as seen in Fig. 8d at all longitudes except the Indian Ocean sector

A pictorial summary of the main coordinated changes that occurred in the "abrupt global climate shift" of the late 1960s is presented in Fig. 11. It is apparent from the above discussion that a significant part of this climate shift can be traced to the tropical Atlantic region and associated precipitation changes in South America and Africa. A closer look at this region is presented in Figs. 12 and 13. Figure 12 shows the SST, precipitation, 850-hPa vector wind, and a vertical section of zonal wind at 5°S for June–August for 1958–67, and Fig. 13 shows changes in the same variables for the period 1976–95. In particular, it is clear that SST has increased in the main region of inflow of low-level air into the Amazon region of South America, as part of the interhemispheric changes in SST described above (there may also be a global warming component). In qualitative terms, this warmer inflow will provide more

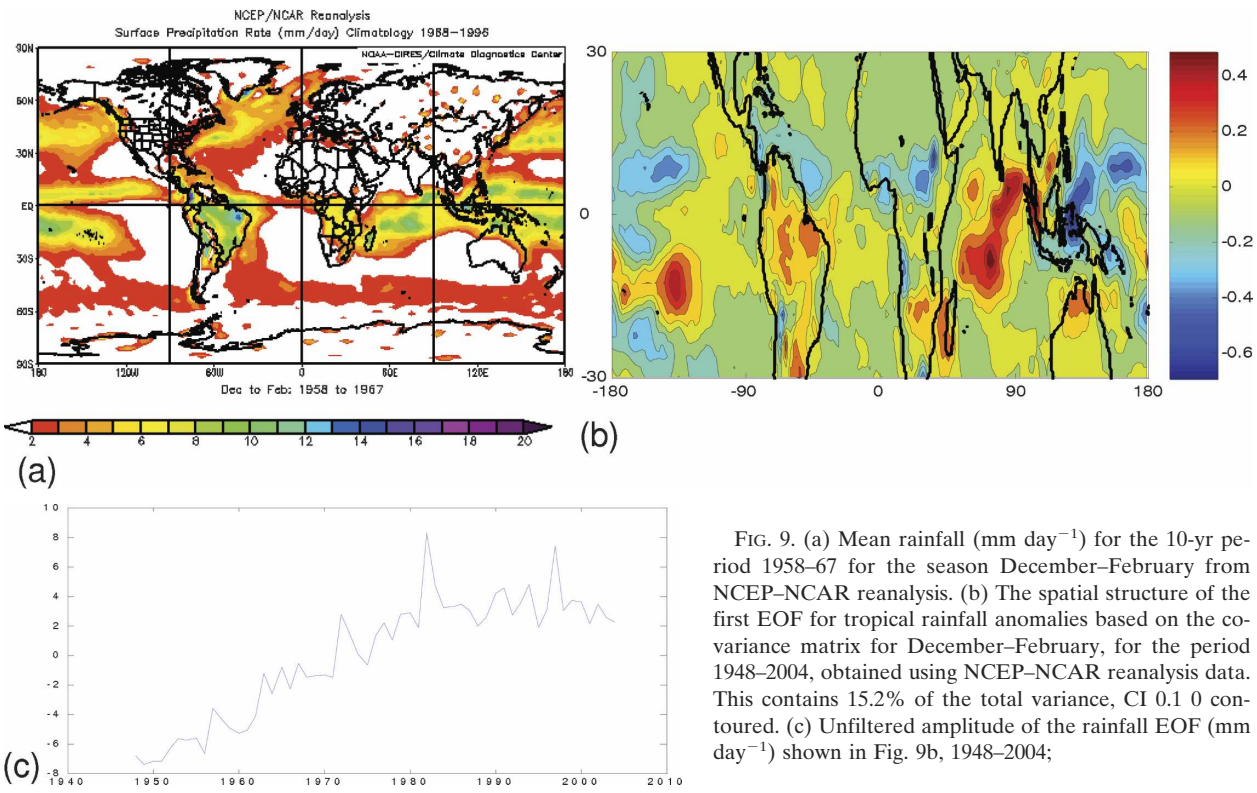

FIG. 9. (a) Mean rainfall (mm day^{-1}) for the 10-yr period 1958–67 for the season December–February from NCEP–NCAR reanalysis. (b) The spatial structure of the first EOF for tropical rainfall anomalies based on the covariance matrix for December–February, for the period 1948–2004, obtained using NCEP–NCAR reanalysis data. This contains 15.2% of the total variance, CI 0.1 0 contoured. (c) Unfiltered amplitude of the rainfall EOF (mm day^{-1}) shown in Fig. 9b, 1948–2004;

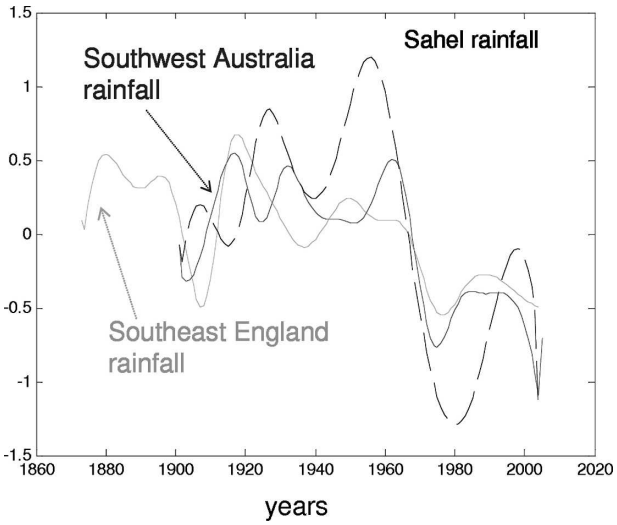

FIG. 10. Rainfall curves for southwestern Western Australia (WA; solid curve) and the African Sahel (dashed curve) for June–August and southeast England rainfall for July–August. The raw data of each time series have been normalized by its respective mean and std dev and low-pass filtered to remove fluctuations with a period less than about 10 yr. Southwest WA data are from the Australian Bureau of Meteorology (see Baines 2005 for details), and Sahel data are from the Hadley Centre.

moisture to the inflowing air over Brazil and hence more net rainfall there. This in turn will cause more latent heating and hence a stronger equatorial Kelvin wave propagating to the east (Gill 1980). Such motion will reduce the westerly low-level inflow to the African rainfall region and will also tend to reduce the upper-level divergence there, causing a reduction of African rainfall. This chain of connections is shown schematically in Fig. 14.

5. Discussion: Possible causes

Various factors have been examined as to their likely contribution to the coordinated climate changes centered on the late 1960s, with the following results.

a. Part of the response to increasing atmospheric concentration of greenhouse gases

This is unlikely as the pattern of quasi-global temperature changes of EOF2, particularly the SST changes, is very unlike the pattern of global warming. The time series is also very different (e.g., compare the AMO time series of Fig. 3b with the global SST warm-

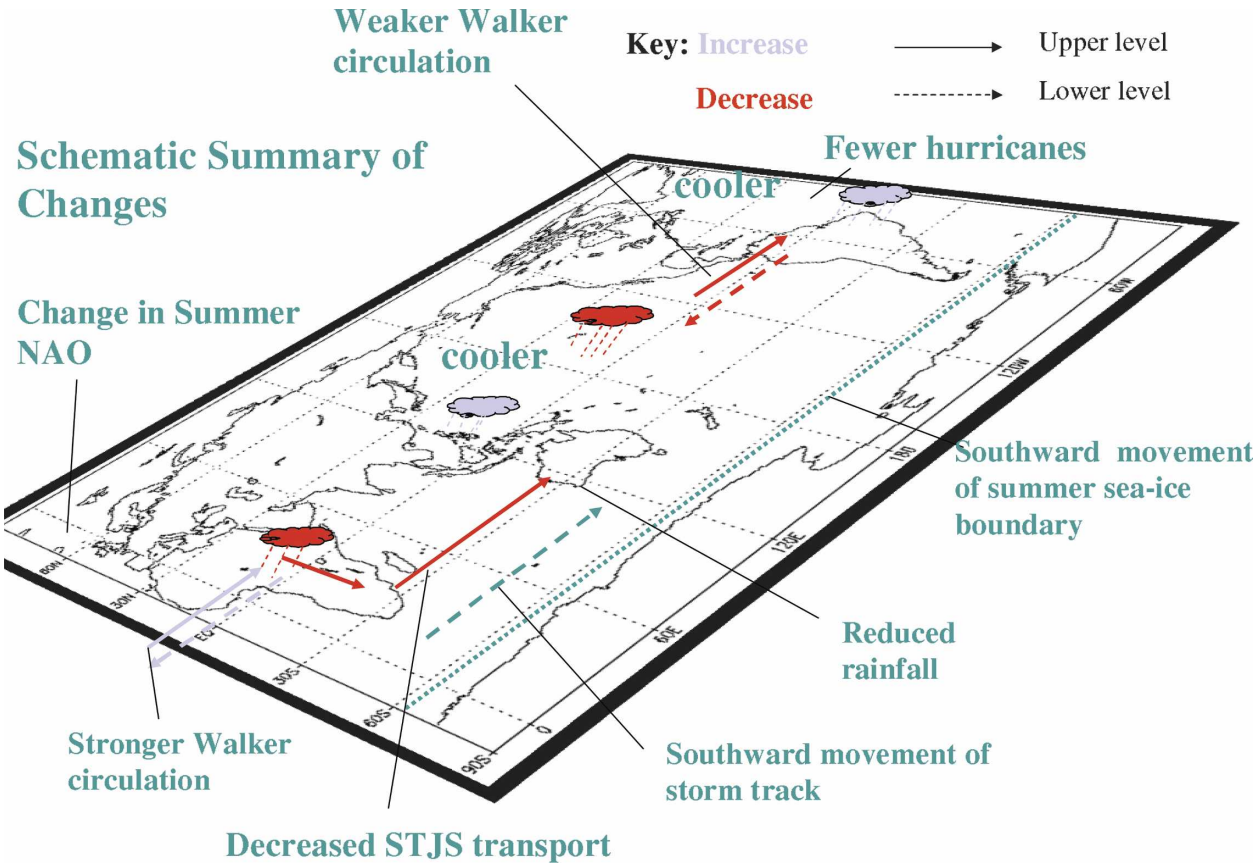

FIG. 11. Schematic depiction of some of the major changes occurring in June–August in the late 1960s. Red (blue) clouds denote decreased (increased) rainfall. Red (blue) arrows denote decreased (increased) winds, with solid arrows denoting upper-tropospheric winds and dashed arrows denoting lower-tropospheric winds; "cooler" refers to SST.

ing series of Fig. 3c). When forced with greenhouse gases alone, coupled models do not reproduce an event of this nature (e.g., Stott et al. 2000) in the late 1960s or early 1970s. Even when all major known forcings are included, the global mean does not show a sharp change (e.g., Stott et al. 2000, 2006).

b. Solar variability

This is very unlikely as solar variability should cause a quasi-global temperature signal of the same sign, not an interhemispheric signal with opposite signs. There is also no evidence of an isolated abrupt change in solar output at this time. The year 1970 coincided with a maximum in the "solar constant" in the 11-yr cycle of total solar irradiance, which has a range of 1 W m^{-2} (peak to peak) or about 0.2 W m^{-2} at the surface, and dominates the reconstructed solar radiation record of the past 50 yr (Lean et al. 1995; Ramaswamy et al. 2001). This periodicity is not evident in the variables studied.

c. The variability of ozone

There is no evidence for this being a significant factor in the 1960s to early 1970s. Ozone has been invoked (Sexton 2001; Thompson and Solomon 2002) as a plausible cause of tropospheric atmospheric circulation changes at high southern latitudes, but these are primarily in the 1980s, coinciding with the deepening of the ozone hole. Such stratospheric influences on the troposphere are mostly confined to the period November to February and associated with the seasonal breakup of the stratospheric vortex, which has negligible signature in June–August.

d. Desertification

This has often been invoked as a possible cause of the long-term drought in the African Sahel. The prevailing evidence now supports the thesis that it is largely caused by several SST patterns that project onto EOF2 of global SST (e.g., Folland et al. 1986; Rowell et al. 1995; Giannini et al. 2003), though a role for land sur-

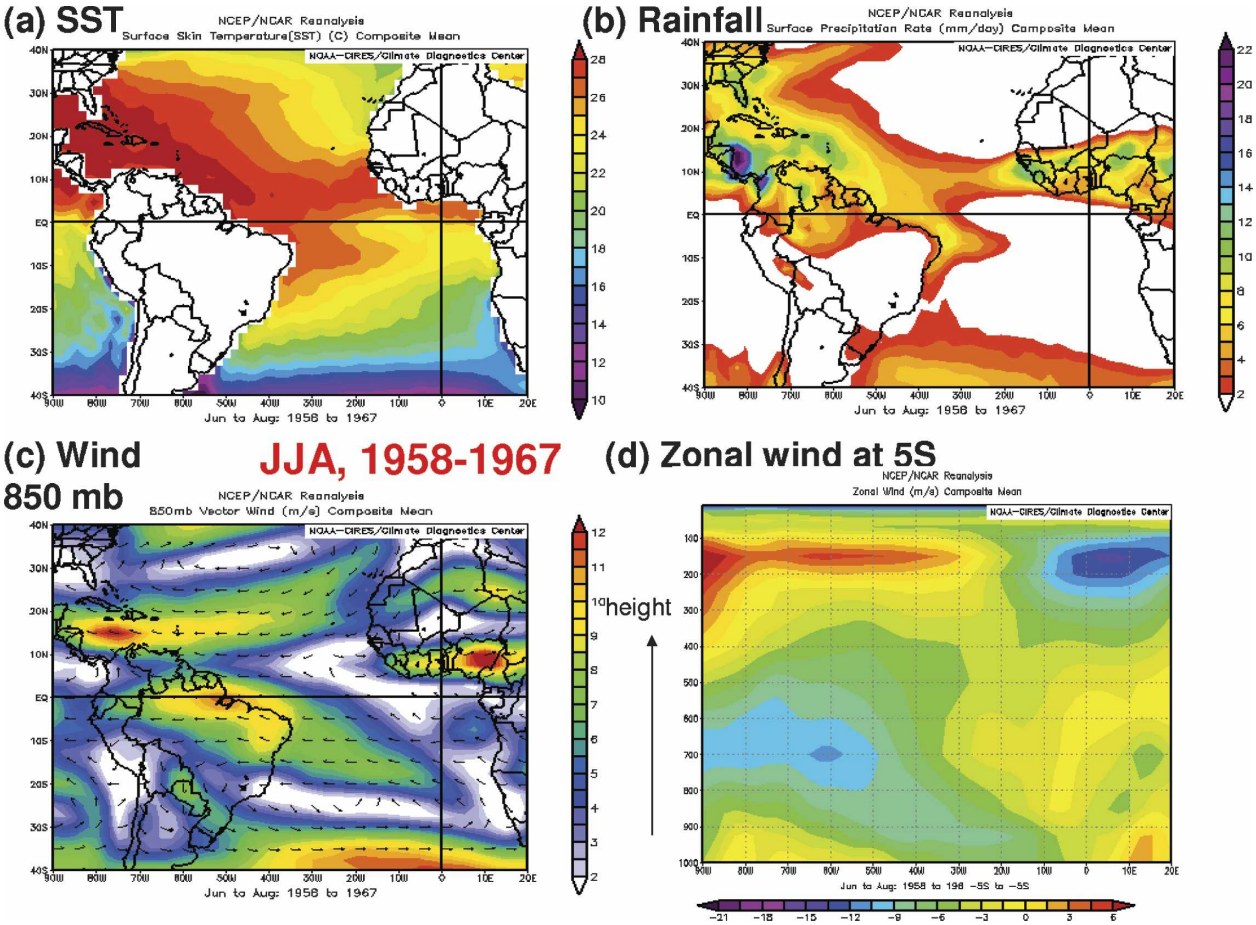

FIG. 12. A closer look at the tropical Atlantic region shown in NCEP reanalysis data for the season June–August for 1958–67 for (a) SST, (b) rainfall, (c) vector winds at 850 hPa, and (d) a vertical section of the zonal wind at 5°S.

face processes is still likely, for example, perhaps through deforestation to the south. However, the observed behavior in the Amazon basin is the opposite of that in the Sahel: the rainfall there has increased in spite of cumulative land clearing (Fearnside 2005) over the past several decades. Although land surface changes are capable of causing changes in rainfall and climate, they are regional and seem unlikely to contribute appreciably to the collective quasi-global phenomena discussed above.

e. Internal variability of the coupled ocean–atmosphere system

In our view this is very likely to be a significant factor. There is substantial evidence of a quasi-interhemispheric fluctuation of temperature variability on a subcentennial time scale centered on the Atlantic extending back to at least 1650 as described by Mann et al. (1998) and Delworth and Mann (2000) using proxy climate data. For the period of overlap, 1871–1980, the phasing of their proxy-based interhemispheric temperature fluctuation (their proxy eigenvector 5) and our SST EOF2 agree well. Furthermore, using evidence from annual growth variations of stalactites in a cave in northwest Scotland, Proctor et al. (2002) find a consistent fluctuation in climate (a combination of temperature and rainfall) on time scales of 50–70 yr between 3000 and 1000 BP, with a slightly longer time scale of 72–94 yr since then.

Such multidecadal fluctuations may occur as part of the natural variability of a chaotic dynamical ocean–atmosphere system, there being no identifiable deterministic cause, as discussed by Delworth and Greatbatch (2000). It is likely that the AMO SST mode may be excited by changes in the transport of the oceanic Atlantic conveyor (Rahmstorf 2002). This possibility is supported by a long 1400-yr control run with the Third Hadley Centre Coupled Ocean–Atmosphere General Circulation Model (HadCM3) by Knight et al. (2005), which indicates peak-to-peak variability of at least 10%

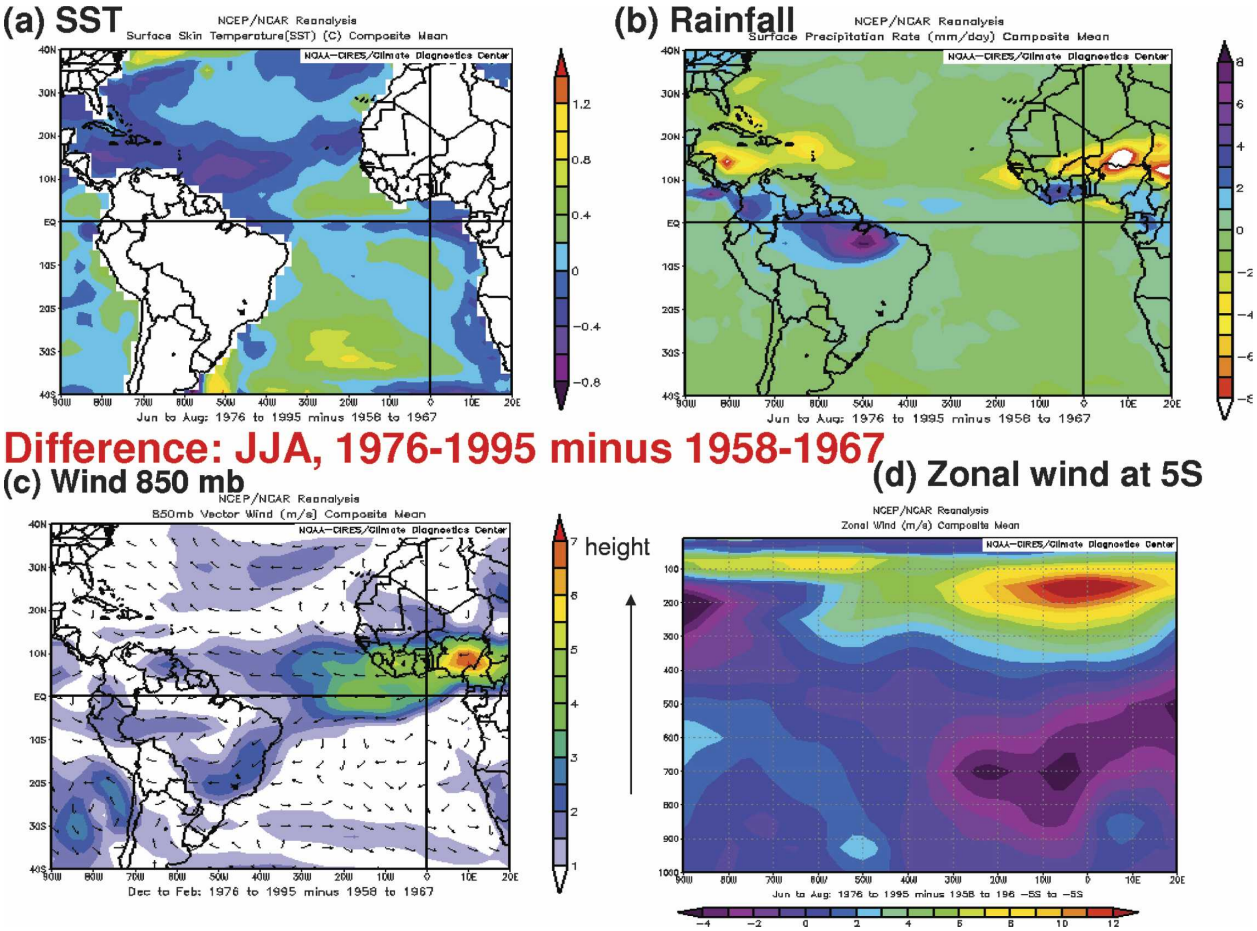

FIG. 13. The same as in Fig. 11, but showing the difference plots for the same four variables between the mean for 1976–95, relative to the mean for 1958–67.

[about 1.5 Sv (1 Sv = 10^6 m^3 s^{-1})] in the Atlantic conveyor transport on time scales near a century. Warming and cooling of the Northern Hemisphere average surface temperature occurred in their model at an average rate of 0.1°C Sv^{-1} and substantially more in North Atlantic Ocean SST. In addition, Latif et al. (2004) show that the Max Planck Institute global climate model (the MPI-OM1 ocean model coupled to the ECHAM5 atmospheric model) produces broadly similar fluctuations involving the thermohaline circulation in a 400-yr control run, though with larger amplitude. Vellinga and Wu (2004) use the HadCM3 control integrations to describe a self-consistent oscillatory mechanism within the North Atlantic Ocean and atmosphere that explains these fluctuations. Delworth and Greatbatch (2002) in fact suggest that the role of chaotic ocean–atmosphere fluctuations could be to enhance, somewhat chaotically in time, the magnitude of smaller quasi-deterministic interdecadal fluctuations. In addition, truly global mechanisms through which the World Ocean might communicate with each other to produce such a thermohaline driven AMO fluctuation have been described by Timmermann et al. (2005).

Knight et al. (2006) note consistently phased fluctuations of the HadCM3 conveyor transport as reflected in North Atlantic SST and observations of surface climate variables, such as Sahel rainfall and northeast Brazil rainfall. The latter (whose main wet season is in boreal spring) is known to be strongly affected by tropical Atlantic SST dipoles centered near the equator on interannual to decadal time scales (Hastenrath and Greischar 1993; Folland et al. 2001a). So a similar, if weaker, response of northeast Brazil rainfall to the AMO pattern is to be expected. In combined observational and model studies using the Third Hadley Centre Coupled Atmospheric Model (HadAM3), Sutton and Hodson (2005) provide evidence of other climatic effects of AMO variations. These include rainfall and pressure at mean sea level fluctuations averaged over the United States and northern Mexico (wetter with lower pressure

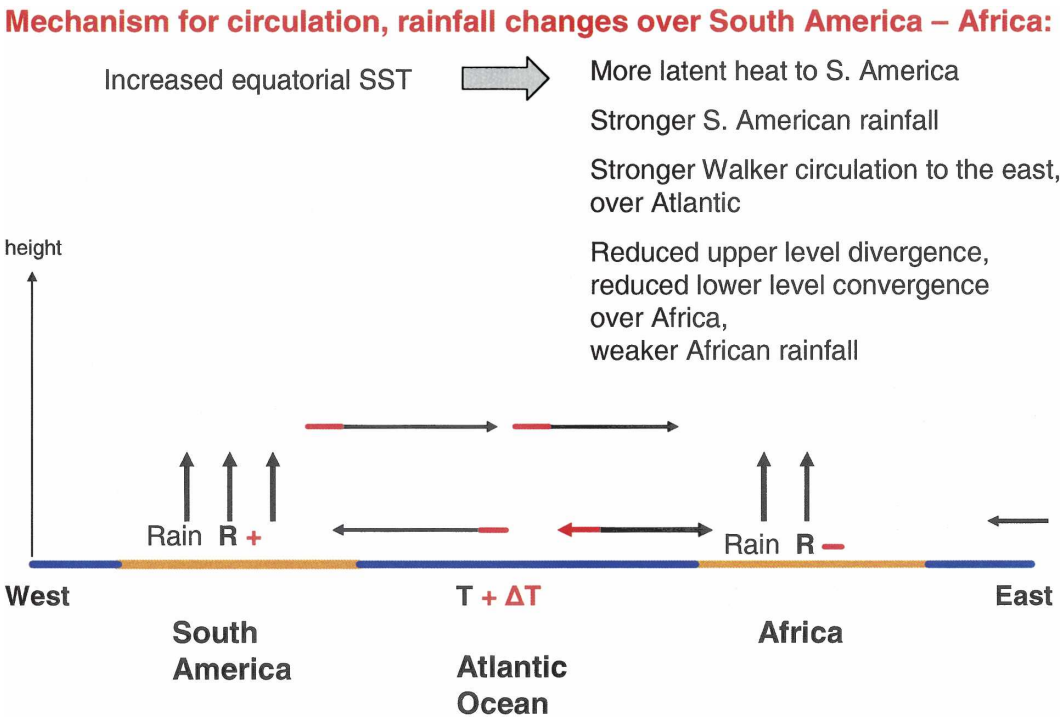

FIG. 14. Schematic diagram of the proposed mechanism for the increase in South American rainfall and the chain of connections causing the decrease in African rainfall for the season June–August due to an increase in SST. Vertical arrows denote rising motion due to convection, and horizontal arrows denote upper and lower zonal flow in the troposphere. Red items denote the changes in 1976–95 quantities relative to 1958–67.

for the warm North Atlantic phase), as well as many of the other influences on North Atlantic climate mentioned previously. Enfield et al. (2001) find similar results for precipitation over the United States, as well as for river flow in an observational study. Finally, a broadly similar interhemispheric SST fluctuation on the shorter time scale near 50 yr is also seen by Delworth and Mann (2000), in a 1000-yr Geophysical Fluid Dynamics Laboratory (GFDL) coupled model control integration.

The idea of a repeated fluctuation is supported by the substantial fluctuations in mean North Atlantic SST shown in Fig. 3c since 1850. There was a possible maximum of SST in the late nineteenth century, a clear minimum near 1910–15, another maximum near 1940, and a strong minimum near 1980. There has been a strong recovery of North Atlantic SST since then. The very rapid warming of about 0.5°C over the last 15 yr is difficult to explain by global warming alone, as global mean SST has risen by only about 0.25°C. However, against the idea of a strong influence of thermohaline circulation reduction on the 1960s climate shift, limited field observations (Bacon 1998) do not show evidence of abrupt monotonic changes in the thermohaline circulation at this time, but this variable is very hard to measure. Kerr (2005) has recently reviewed the latest evidence on the topic.

f. The effect of anthropogenic sulfate aerosols

Anthropogenic aerosols affect radiation reaching the surface both directly and indirectly (Haywood and Boucher 2000; Houghton et al. 2001). The indirect effect occurs because aerosols act as cloud condensation nuclei (CCN) and thereby increase cloud albedo and lifetime. Through their role as CCN, they may also suppress rainfall (Rosenfeld 2000; Ramanathan et al. 2001) and hence alter the distribution of latent heat release. The direct effect causes a net scattering of solar radiation to space and therefore a surface cooling. The magnitudes of these effects (particularly the indirect effects) and the temporal and spatial distribution of the various types of aerosols are all still uncertain, but evidence is mounting that they are significant in global terms. Thus, recent modeling studies have suggested that aerosol-forced changes in atmospheric circulation may have large impacts on rainfall in tropical and subtropical regions (Rotstayn and Lohmann 2002; Menon et al. 2002). Furthermore, by including the best estimates of time-varying direct and indirect sulfate aerosol effects with increasing greenhouse gases and natural

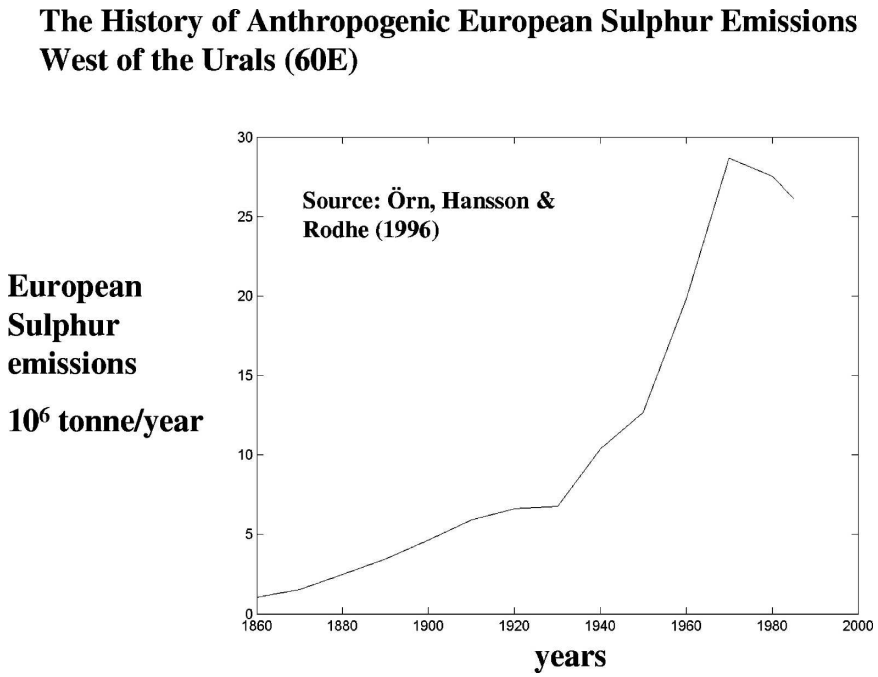

FIG. 15. The history of anthropogenic European sulfur emissions west of the Urals (60°E), from Örn et al. (1996).

solar and volcanic forcings, Stott et al. (2000) were able to reproduce the global temperature variations since 1861 with considerable fidelity using the HadCM3 coupled model, including the weak global cooling in the 1960s to early 1970s. The latter arose mostly from the addition of anthropogenic sulfate aerosols in the Northern Hemisphere, particularly over the United States and Europe. This result has been extended recently to two other models by Stott et al. (2006).

Of the various types of aerosol, sulfate has been studied most extensively. The main anthropogenic source of sulfate is the oxidation of sulfur dioxide emitted when sulfur-containing fossil fuels are burned. European and North American emissions of sulfur dioxide increased massively after 1950, peaking in the mid-1970s, as illustrated in Fig. 15. Rotstayn and Lohmann (2002) describe results from two runs of the Commonwealth Scientific and Industrial Research Organisation (CSIRO) atmospheric model with a mixed-layer ocean, one using preindustrial (PI) emissions of sulfur and the other using present-day (PD) emissions, which correspond to the mid-1980s. The difference in the distribution of sulfate aerosol between these two runs is shown in Fig. 16a. The sulfate aerosol influenced cloud albedo and lifetime in these runs, but the direct radiative effect of sulfate was excluded. Thus, the difference between the two runs gives an estimate of the climatic response to the indirect effects of sulfate aerosol. The difference in equilibrium annual mean near-surface air temperature between the two runs is shown in Fig. 16b. Clearly, the Northern Hemisphere has cooled relative to the Southern Hemisphere in the PD run. A comparison with the observations in Fig. 3a shows a general similarity, the principal exception being that the Southern Hemisphere surface is observed to warm, whereas the sulfates cool almost everywhere. This warming is very likely to be due to several factors that are not represented in the model runs, particularly greenhouse warming, but also the possible warming effect of absorbing aerosols.

Stott et al. (2006) show that when observational constraints are imposed on the climate sensitivity of several coupled models forced in a similar way to the experiments of Stott et al. (2000), a clear interhemispheric signal of relative cooling of the Northern Hemisphere and relative warming of the Southern Hemisphere occurs. The relative cooling starts about 1950 and is almost coincident with the 1960s climate shift. The relative coldness of the Northern Hemisphere peaks around 1975, with the Northern Hemisphere relatively cooler at around 0.2°C than the Southern, followed by a relative warming of the Northern Hemisphere in 1995 of about 0.2°C. The changes are quite similar in magnitude and phase in all three models. The phasing of the changes is quite similar to SST EOF2 over the same period and the magnitude of the relative hemispheric

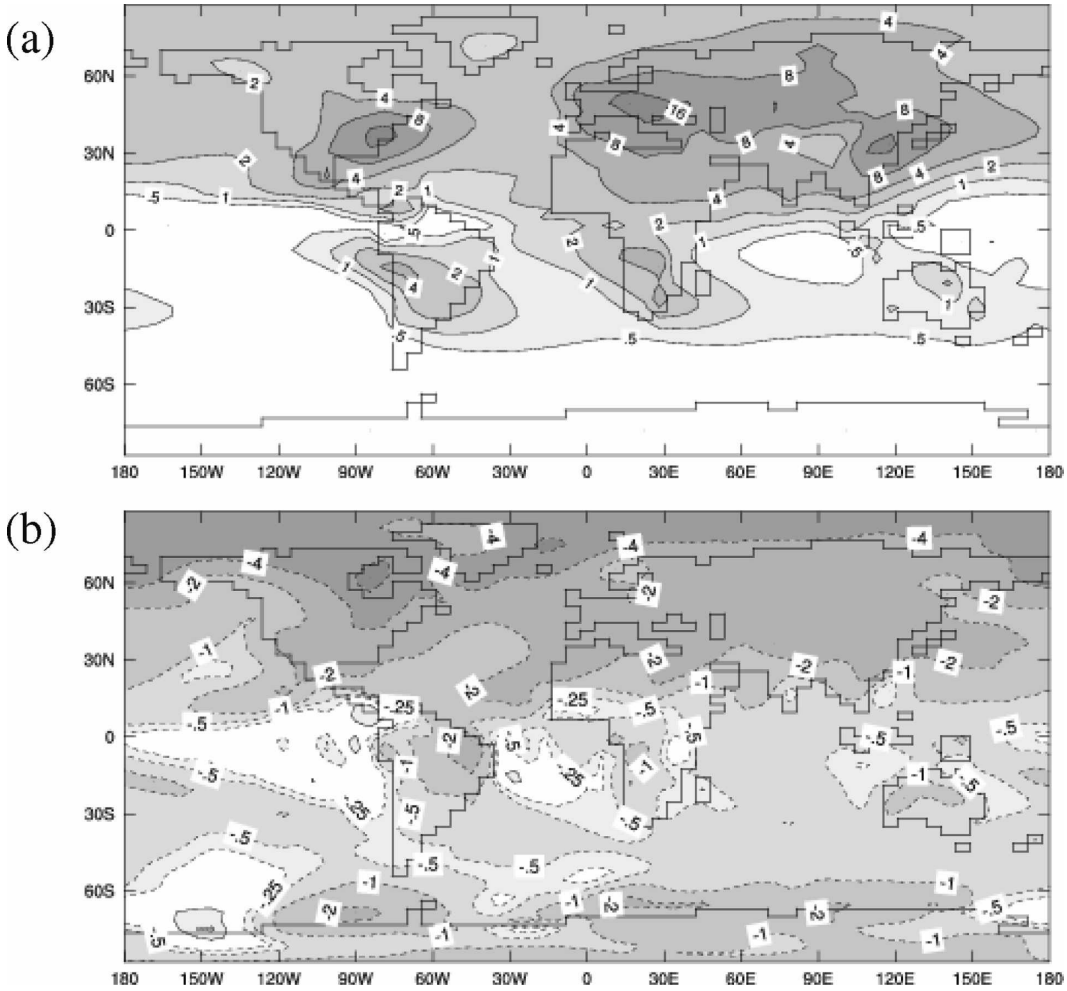

FIG. 16. (a) Difference between the annual mean sulfate column burden for present day (mg m^{-2}, circa 1985) and preindustrial conditions. (b) Difference in annual mean near-surface air temperature between two runs with a CSIRO atmospheric model with a mixed layer ocean, one (preindustrial) without sulfates and the other (present day) with the concentration distribution shown in (a), from Rotstayn and Lohmann (2002).

surface temperature change is quite similar to observations (see Folland et al. 2001b,c). However, it is not possible from these results to deduce the forced changes in hemispheric or regional SST.

A cooling of the Northern Hemisphere oceans relative to the Southern Hemisphere oceans has been shown to cause a decrease in rainfall in the African Sahel (Folland et al. 1986; Rowell et al. 1995). Rowell et al. (1992) relate this (comparing some very dry with very wet years) to both a southward shift of the intertropical convergence zone and more particularly a reduction in its intensity, reducing the moisture flux convergence into the Sahel. The latter is consistent with a weakening of the associated Hadley circulation seen in Fig. 4b. The difference between the rainfall in the PD and PI runs of Rotstayn and Lohmann (2002) (Fig. 17a) also shows a decrease there and prompted Rotstayn and Lohmann to postulate the indirect effects of sulfate aerosol as a cause of drought in the Sahel. More generally, the surface temperature response to sulfate aerosol forcing is seen to affect the global pattern of tropical rainfall. For comparison, the observed differences in rainfall between the decades 1971–80 and 1958–67 are shown in Fig. 17b. There are some differences between the observed and simulated rainfall changes, principally in the Southeast Asian region, but there are many similarities. In general, for both, the northern Tropics are dryer and the southern Tropics are wetter, and this includes in particular the African Sahel and the Amazon basin. The causes of the changes in the Hadley circulation and the subtropical jet stream then follow.

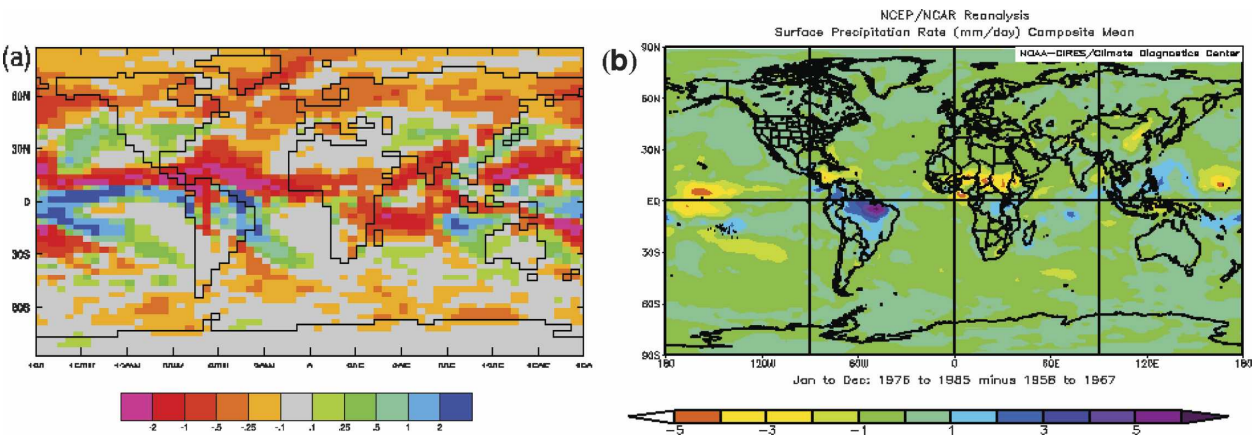

FIG. 17. (a) Difference in annual mean precipitation (mm day^{-1}) between the present-day and preindustrial runs as depicted in Fig. 15, from Rotstayn and Lohmann (2002). (b) Observed annual mean rainfall for the decade 1976–85 minus that for the decade 1958–67 from NCEP–NCAR reanalysis.

The reasons why cooling of the Northern Hemisphere relative to the Southern Hemisphere should decrease the tropical rainfall there are intuitively at least partly obvious: the reduction in temperature, particularly sea surface temperature, tends to shift the intertropical convergence zone southward in the wet season as this follows the absolute SST maximum. Reasons for reductions in the moisture flux convergence over the Sahel when a relatively cold Northern Hemisphere occurs are likely to relate in part to the lower water vapor content of a colder atmosphere. For Sahel, a cooler Mediterranean typically associated with a cold Northern Hemisphere has been shown by Rowell (2003) to result in air crossing to the Sahara from the Mediterranean to have less moisture content.

It was noted above that the observed "abrupt changes" in rainfall across the late 1960s were smaller in magnitude in DJF than in JJA (cf. Figs. 4 and 6 with Fig. 8). There are also seasonal variations in the aerosol radiative forcing, and estimated magnitudes of the indirect effect from the CSIRO model are shown in Table 2. This difference is mainly due to the large seasonal variations in solar radiation. Clearly, the interhemispheric difference is larger in JJA than in DJF, consistent with the observed changes in rainfall.

TABLE 2. Estimated magnitudes of the first indirect effect of aerosol radiative forcing from the CSIRO coupled model corresponding to the mid-1980s, compared to preindustrial conditions (data provided by L. Rotstayn, personal communication).

	JJA	DJF
Northern Hemisphere	−2.87	−1.21 W m^{-2}
Southern Hemisphere	−0.78	−0.50

6. Conclusions

A number of significant variables of the atmospheric circulation underwent large coordinated changes over about a decade centered on the late 1960s. These effects were strongest in the season June–August. The approximate order of influence is thought to be as follows. An interhemispheric difference in SST developed, with the Northern Hemisphere becoming distinctly colder and the Southern Hemisphere slightly warmer. This was associated with decreases in tropical rainfall in the African Sahel and the central Pacific and increase in the Amazon basin, giving corresponding changes in the Hadley and Walker circulations and hence also in the subtropical jet stream. Most of these changes are linked dynamically. Model studies show that the interhemispheric change in SST can cause changes in tropical rainfall (a cooler Northern Hemisphere results in reduced tropical rainfall north of the equator in the wet season and increased rainfall south of it) that are qualitatively consistent with those observed on an annual basis. Such changes are likely in part to relate to latitudinal shifts in the intertropical convergence zone, as well as changes in its intensity. These changes in rainfall imply corresponding changes in the latent heat released in the same regions and hence cause changes in the Hadley circulations (to the south in JJA) and Walker circulations (to the east) consistent with simple dynamical models of tropical heating. These changes in turn affect the westerlies in midlatitudes, and hence the development of synoptic features, changes in which affect the weather in these regions. The list of these 1960s changes and their consequences is still far from complete. A depiction of the mechanism by which the Bra-

zilian rainfall increase is connected with the Sahel drought is shown in Fig. 14.

It is suggested that the changes centered on the 1960s may be largely due to (a) a reduction in the strength of the global thermohaline circulation and (b) a coincident increase in sulfate aerosol concentration in the Northern Hemisphere after 1945, particularly concentrated in the Atlantic sector. The likely importance of the natural variations in the global thermohaline circulation is shown by Delworth and Mann (2000), Latif et al. (2004), and particularly by Knight et al. (2005, 2006). A repeated warming of the North Atlantic region relative to the South Atlantic region on the multidecadal time scale is consistent with evidence from four centuries of proxy temperature data as shown by Mann et al. (1998), the observational and modeling studies of Delworth and Mann (2000), and a very persistent climate fluctuation on the same time scale affecting Scotland as shown by Proctor et al. (2002).

There is a considerable amount of climate prediction research using many climate models that consistently suggests an impact of global warming on the thermohaline circulation so as to slow it (assessed in Cubasch et al. 2001). Recently Bryden et al. (2005) have claimed to detect a recent slowdown of the thermohaline circulation from sparsely sampled oceanographic data. However, Knight et al. (2005), based on model results and recent observed SST changes and after allowing for anthropogenic effects on SST, argue in favor of an increase in the thermohaline circulation strength associated with the recent sharp warming of North Atlantic SST. This conclusion is supported by Latif et al. (2006). Thus we conclude that there is no convincing evidence of a slowing effect on the thermohaline circulation due to anthropogenic effects on climate. In fact we consider a recent increase is more likely. However, a sharp decline in the thermohaline circulation in the next few decades due to a combination of natural and anthropogenic effects is thought likely by Knight et al (2005).

The influence of anthropogenic sulfate aerosols on regional or hemispheric climate is particularly supported by the modeling studies of Rotstayn and Lohmann (2002) and Stott et al. (2006). The observed distribution of aerosols in space and time is consistent with the observed changes in SST, which cause the observed changes in rainfall and hence the atmospheric circulation changes, as stated above. It is also consistent with the observed decrease in global surface temperature from 1945 to 1970, which was almost entirely concentrated in the Northern Hemisphere. It is also consistent with the observation that the late 1960s changes are strongest in the season June–August, when sunlight is strongest in the Northern Hemisphere and the global radiative impact of aerosols is largest.

It must be emphasized that this AMO-related climate shift is a separate phenomenon from the ENSO-like climate shift of the Pacific dated around 1975 and described by, among others, Zhang et al. (1997) and Garreaud and Battisti (1999). This is likely related in part to variations in the interdecadal Pacific oscillation/Pacific decadal oscillation, which changed phase at the same time (Folland et al. 2002). Connections between the two phenomena may exist, however, as mentioned in Knight et al. (2006).

Finally, we conclude that to fully understand, and predict, changes of regional climates, such as were seen in the 1960s shift, and may be occurring now, quantifying the relative influences of modes of regional natural variability and different types of anthropogenic forcing is very important. Thus, it is particularly likely that one of the indexes we show in Fig. 1, south Greenland temperature, is currently being comparably influenced by the effects of both global warming and the natural component of the Atlantic multidecadal oscillation.

Acknowledgments. The authors would like to acknowledge discussions and input from Leon Rotstayn, Ian Smith, and Wenju Cai of CSIRO Atmospheric Research, who contributed to this work in the early stages, and discussions with Adam Scaife and Jeff Knight of the Hadley Centre. The first author would like to acknowledge support from the Leverhulme Trust, as the paper was essentially completed during tenure of a Leverhulme Visiting Professorship at Bristol University. The second author wishes to thank John Kennedy and Andrew Colman for help with diagrams and also acknowledges support from the U.K. Government Meteorological Research Program.

REFERENCES

Alley, R. B., and Coauthors, Eds., 2002: *Abrupt Climate Change: Inevitable Surprises*. National Academy Press, 230 pp.

——, and Coauthors, 2003: Abrupt climate change. *Science,* **299,** 2005–2010.

Ansell, T. J., and Coauthors, 2006: Daily mean sea level pressure reconstructions for the European–North Atlantic region for the period 1850–2003. *J. Climate,* **19,** 2717–2742.

Bacon, S., 1998: Decadal variability in the outflow from the Nordic seas to the deep Atlantic Ocean. *Nature,* **394,** 871–874.

Baines, P. G., 2005: Long-term variations in winter rainfall of Southwest Australia and the African monsoon. *Aust. Meteor. Mag.,* **54,** 91–102.

Brohan, P., J. J. Kennedy, I. Harris, S. F. B. Tett, and P. D. Jones, 2006: Uncertainty estimates in regional and global observed temperature changes: A new data set from 1850. *J. Geophys. Res.,* **111,** D12106, doi:10.1029/2005JD006548.

Bryden, H. L., H. R. Longworth, and S. A. Cunningham, 2005:

Slowing of the Atlantic meridional overturning circulation at 25°N. *Nature,* **438,** 655–657.

Cai, W., and P. Whetton, 2001: Modes of SST variability and the fluctuation of global mean temperature. *Climate Dyn.,* **17,** 889–901.

Chylek, P., M. K. Dubey, and G. Lesins, 2006: Greenland warming of 1920–1930 and 1995–2005. *Geophys. Res. Lett.,* **33,** L11707, doi:10.1029/2006GL026510.

Cubasch, U., G. A. Meehl, G. J. Boer, M. Dix, A. Noda, C. A. Senior, S. Raper, and K. S. Yap, 2001: Projections of future climate change. *Climate Change 2001: The Scientific Basis,* J. T. Houghton et al., Eds., Cambridge University Press, 99–181.

Dai, A., P. J. Lamb, K. Trenberth, M. Hulme, P. D. Jones, and P. Xie, 2004: The recent Sahel drought is real. *Int. J. Climatol.,* **24,** 1323–1331.

de la Mare, W. K., 1997: Abrupt mid-twentieth-century decline in Antarctic sea-ice extent from whaling records. *Nature,* **389,** 57–60.

Delworth, T. L., and R. J. Greatbatch, 2000: Multidecadal thermohaline circulation variability driven by atmospheric surface flux forcing. *J. Climate,* **13,** 1481–1495.

——, and M. E. Mann, 2000: Observed and simulated multidecadal variability in the Northern Hemisphere. *Climate Dyn.,* **16,** 661–676.

Enfield, D. B., A. M. Mestas-Nunez, and P. J. Trimble, 2001: The Atlantic Multidecadal Oscillation and its relation to rainfall and river flows in the continental US. *Geophys. Res. Lett.,* **28,** 2077–2080.

Fearnside, P. M., 2005: Deforestation in Brazilian Amazonia: History, rates and consequences. *Conserv. Biol.,* **19,** 680–688.

Folland, C. K., T. N. Palmer, and D. E. Parker, 1986: Sahel rainfall and worldwide sea temperatures, 1901–1985. *Nature,* **320,** 602–604.

——, D. E. Parker, A. Colman, and R. Washington, 1999: Large scale modes of ocean surface temperature since the late nineteenth century. *Beyond El-Niño: Decadal and Interdecadal Climate Variability,* A. Navarra, Ed., Springer-Verlag, 73–102.

——, A. W. Colman, D. P. Rowell, and M. K. Davey, 2001a: Predictability of Northeast Brazil rainfall and real-time forecast skill, 1987–98. *J. Climate,* **14,** 1937–1958.

——, and Coauthors, 2001b: Observed climate variability and change. *Climate Change 2001: The Scientific Basis,* J. T. Houghton et al., Eds., Cambridge University Press, 99–181.

——, and Coauthors, 2001c: Global temperature change and its uncertainties since 1861. *Geophys. Res. Lett.,* **28,** 2621–2624.

——, J. A. Renwick, M. J. Salinger, and A. B. Mullan, 2002: Relative influences of the Interdecadal Pacific Oscillation and ENSO on the South Pacific Convergence Zone. *Geophys. Res. Lett.,* **29,** 1643, doi:10.1029/2001GL014201.

Garreaud, R. D., and D. S. Battisti, 1999: Interannual (ENSO) and Interdecadal (ENSO-like) variability in the Southern Hemisphere tropospheric circulation. *J. Climate,* **12,** 2113–2123.

Giannini, A., R. Saravanan, and P. Chang, 2003: Oceanic forcing of Sahel rainfall on interannual to interdecadal time scales. *Science,* **302,** 1027–1030.

Gill, A. E., 1980: Some simple solutions for heat-induced tropical circulation. *Quart. J. Roy. Meteor. Soc.,* **106,** 447–462.

——, 1982: *Atmosphere–Ocean Dynamics.* Academic Press, 662 pp.

Goldenberg, S. B., C. W. Landsea, A. M. Mestas-Nuñez, and W. M. Gray, 2001: The recent increases in Atlantic hurricane activity: Causes and implications. *Science,* **293,** 474–479.

Greatbatch, R. J., and P.-P. Rong, 2006: Discrepancies between different Northern Hemisphere summer atmospheric data products. *J. Climate,* **19,** 1261–1273.

Hastenrath, S., and L. Greischar, 1993: Circulation mechanisms related to northeast Brazil rainfall anomalies. *J. Geophys. Res.,* **98** (D3), 5093–5102.

Haywood, J., and O. Boucher, 2000: Estimates of the direct and indirect radiative forcing due to tropospheric aerosols: A review. *Rev. Geophys.,* **38,** 513–543.

Houghton, J. T., Y. Ding, D. J. Griggs, M. Noguer, P. J. van der Linden, X. Dai, K. Maskell, and C. A. Johnson, Eds., 2001: *Climate Change 2001: The Scientific Basis.* Cambridge University Press, 881 pp.

Huang, N. E., and Coauthors, 1998: The empirical mode decomposition and the Hilbert spectrum for nonlinear and nonstationary time series analysis. *Proc. Roy. Soc. A,* **454,** 903–995.

——, Z. Shen, and S. S. Long, 1999: A new view of nonlinear water waves: The Hilbert Spectrum. *Annu. Rev. Fluid Mech.,* **31,** 417–457.

Hurrell, J. W., and C. K. Folland, 2002: The relationship between tropical Atlantic rainfall and the summer circulation over the North Atlantic. *CLIVAR Exchanges,* No. 25, International CLIVAR Project Office, Southampton, United Kingdom, 52–54.

——, Y. Kushnir, G. Ottersen, and M. Visbeck, 2003: An overview of the North Atlantic Oscillation. *The North Atlantic Oscillation: Climatic Significance and Environmental Impact, Geophys. Monogr.,* Vol. 134, Amer. Geophys. Union, 1–35.

IOCI, 2002: Climate variability and change in south west Western Australia. Indian Ocean Climate Initiative Panel Tech. Rep., Perth, Australia, 34 pp.

Kalnay, E., and Coauthors, 1996: The NCEP/NCAR 40-Year Reanalysis Project. *Bull. Amer. Meteor. Soc.,* **77,** 437–471.

Kerr, R. A., 2005: Atlantic climate pacemaker for millennia past, decades hence? *Science,* **309,** 41–43.

Kistler, R., and Coauthors, 2001: The NCEP–NCAR 50-Year Reanalysis: Monthly means CD-ROM and documentation. *Bull. Amer. Meteor. Soc.,* **82,** 247–267.

Knaff, J. A., 1997: Implications of summertime sea level pressure anomalies in the tropical Atlantic region. *J. Climate,* **10,** 789–804.

Knight, J. R., R. J. Allan, C. K. Folland, M. Vellinga, and M. E. Mann, 2005: A signature of persistent natural thermohaline circulation cycles in observed climate. *Geophys. Res. Lett.,* **32,** L20708, doi:10.1029/2005GL024233.

——, C. K. Folland, and A. A. Scaife, 2006: Climatic impacts of the Atlantic Multidecadal Oscillation. *Geophys. Res. Lett.,* **33,** L17706, doi:10.1029/2006GL026242.

Kushnir, Y., 1994: Interdecadal variations in North Atlantic sea surface temperature and associated atmospheric conditions. *J. Climate,* **7,** 141–157.

Landsea, C. W., R. A. Pielke, A. M. Mestas-Nuñez, and J. A. Knaff, 1999: Atlantic basin hurricanes: Indices of climatic changes. *Climatic Change,* **42,** 89–129.

Latif, M., and Coauthors, 2004: Reconstructing, monitoring, and predicting multidecadal-scale changes in the North Atlantic thermohaline circulation with sea surface temperature. *J. Climate,* **17,** 1605–1614.

——, C. Boning, J. Willebrand, A. Biastoch, J. Dengg, N. Keenly-

side, G. Madec, and U. Schweckendiek, 2006: Is the thermohaline circulation changing? *J. Climate,* **19,** 4631–4637.

Lau, K.-M., and P. J. Sheu, 1990: Teleconnections in global rainfall anomalies: Seasonal to inter-decadal time scales. *Teleconnections Linking Worldwide Climate Anomalies,* M. Glantz, W. Katz, and N. Nicholls, Eds., Cambridge University Press, 227–256.

Lean, J., J. Beer, and R. Bradley, 1995: Reconstruction of solar irradiance since 1610: Implications for climate change. *Geophys. Res. Lett.,* **22,** 3195–3198.

Mann, M. E., and J. Park, 1994: Global-scale modes of surface temperature variability on interannual to century timescales. *J. Geophys. Res.,* **99,** 25 819–25 833.

——, R. S. Bradley, and M. K. Hughes, 1998: Global-scale temperature patterns and climatic forcing over the past six centuries. *Nature,* **392,** 779–787.

Mantua, N. J., S. R. Hare, Y. Zhang, J. M. Wallace, and R. C. Francis, 1997: A Pacific interdecadal climate oscillation with impacts on salmon production. *Bull. Amer. Meteor. Soc.,* **78,** 1069–1079.

Menon, S., J. Hansen, L. Nazarenko, and Y. Luo, 2002: Climate effects of black carbon aerosols in China and India. *Science,* **197,** 2250–2253.

Örn, G., U. Hansson, and H. Rodhe, 1996: Historical worldwide emissions of anthropogenic sulphur: 1860–1985. Rep. CM-91, Department of Meteorology, Stockholm University, Stockholm, Sweden, 16 pp.

Parker, D. E., P. D. Jones, C. K. Folland, and A. Bevan, 1994: Interdecadal changes of surface temperature since the late 19th century. *J. Geophys. Res.,* **99,** 14 377–14 399.

Phillips, N. A., 1954: Energy transformations and meridional circulations associated with simple baroclinic waves in a two-level, quasi-geostrophic model. *Tellus,* **6,** 273–286.

Power, S., T. Casey, C. K. Folland, A. Colman, and V. Mehta, 1999: Inter-decadal modulation of the impact of ENSO on Australia. *Climate Dyn.,* **15,** 319–323.

Proctor, C. J., A. Baker, and W. L. Barnes, 2002: A three thousand year record of North Atlantic climate. *Climate Dyn.,* **19,** 449–454.

Rahmstorf, S., 2002: Ocean circulation and climate during the past 120,000 years. *Nature,* **419,** 207–214.

Ramanathan, V., P. J. Crutzen, J. T. Kiehl, and D. Rosenfeld, 2001: Aerosols, climate and the hydrological cycle. *Science,* **294,** 2119–2124.

Ramaswamy, V., and Coauthors, 2001: Radiative forcing of climate change. *Climate Change 2001: The Scientific Basis,* J. T. Houghton et al., Eds., Cambridge University Press, 349–416.

Rayner, N. A., E. B. Horton, D. E. Parker, C. K. Folland, and R. B. Hackett, 1996: Version 2.2 of the global sea-ice and sea surface temperature data set, 1903–1994. Climate Research Tech. Note CRTN74, Hadley Centre, Met Office, Bracknell, United Kingdom, 35 pp.

——, D. E. Parker, E. B. Horton, C. K. Folland, L. V. Alexander, D. P. Rowell, E. C. Kent, and A. Kaplan, 2003: Global analyses of sea surface temperature, sea ice, and night marine air temperature since the late nineteenth century. *J. Geophys. Res.,* **108,** 4407, doi:10.1029/2002JD002670.

——, P. Brohan, D. E. Parker, C. K. Folland, J. J. Kennedy, M. Vanicek, T. J. Ansell, and S. F. B. Tett, 2006: Improved analyses of changes and uncertainties in sea surface temperature measured in situ since the mid-nineteenth century: The HadSST2 data set. *J. Climate,* **19,** 446–469.

Rosenfeld, D., 2000: Suppression of rain and snow by urban and industrial pollution. *Science,* **287,** 1793–1796.

Rotstayn, L. D., and U. Lohmann, 2002: Tropical rainfall trends and the indirect aerosol effect. *J. Climate,* **15,** 2103–2116.

Rowell, D. P., 2003: The impact of Mediterranean SSTs on the Sahelian rainfall season. *J. Climate,* **16,** 849–862.

——, C. K. Folland, K. Maskell, J. A. Owen, and M. N. Ward, 1992: Modeling the influence of global sea surface temperature on the variability and predictability of seasonal Sahel rainfall. *Geophys. Res. Lett.,* **19,** 905–908.

——, ——, ——, and M. N. Ward, 1995: Variability of summer rainfall over tropical North Africa (1906–92): Observations and modelling. *Quart. J. Roy. Meteor. Soc.,* **121,** 669–704.

Sexton, D. M. H., 2001: The effect of stratospheric ozone depletion on the phase of the Antarctic Oscillation. *Geophys. Res. Lett.,* **28,** 3697–3700.

Smith, I. N., P. McIntosh, T. J. Ansell, C. J. C. Reason, and K. McInnes, 2000: Southwest Western Australian winter rainfall and its association with Indian Ocean climate variability. *Int. J. Climatol.,* **20,** 1913–1930.

Stott, P. A., S. F. B. Tett, G. S. Jones, M. R. Allen, J. F. B. Mitchell, and G. J. Jenkins, 2000: External control of 20th century temperature by natural and anthropogenic forcings. *Science,* **290,** 2133–2137.

——, J. F. B. Mitchell, M. R. Allen, T. L. Delworth, J. M. Gregory, G. A. Meehl, and B. D. Santer, 2006: Observational constraints on past attributable warming and predictions of future global warming. *J. Climate,* **19,** 3055–3069.

Sutton, R. T., and D. L. R. Hodson, 2005: Atlantic Ocean forcing of North American and European summer climate. *Science,* **309,** 115–118.

Thompson, D. W. J., and S. Solomon, 2002: Interpretation of recent Southern Hemisphere climate change. *Science,* **296,** 895–899.

Timbal, B., J. M. Arblaster, and S. Power, 2006: Attribution of the late-twentieth-century rainfall decline in Southwest Australia. *J. Climate,* **19,** 2046–2062.

Timmermann, A., S.-I. An, U. Krebs, and H. Goosse, 2005: ENSO suppression due to weakening of the North Atlantic thermohaline circulation. *J. Climate,* **18,** 3122–3139.

Trenberth, K. E., D. P. Stepaniak, and J. M. Caron, 2000: The global monsoon as seen through the divergent atmospheric circulation. *J. Climate,* **13,** 3969–3993.

Uppala, S. M., and Coauthors, 2005: The ERA-40 re-analysis. *Quart. J. Roy. Meteor. Soc.,* **131,** 2961–3012.

Vellinga, M., and P. Wu, 2004: Low-latitude freshwater influence on centennial variability of the Atlantic thermohaline circulation. *J. Climate,* **17,** 4498–4511.

Zhang, Y., J. M. Wallace, and D. S. Battisti, 1997: ENSO-like interdecadal variability: 1900–1993. *J. Climate,* **10,** 1004–1020.